Shape, rheology and emplacement times of small martian shield volcanoes

D. Baratoux [a,*], P. Pinet [a], M.J. Toplis [a], N. Mangold [b], R. Greeley [c], A.R. Baptista [d,1]

[a] Observatoire Midi-Pyrénées, Laboratoire Dynamique Terrestre et Planétaire, UMR 5562, Université Paul Sabatier, Toulouse, France
[b] Laboratoire de Planétologie et Géodynamique, Nantes University, UMR CNRS 6612, Nantes, France
[c] School of Earth and Space Exploration, Arizona State University, Box 871404, Tempe, AZ, USA
[d] Institut de Physique du Globe de Paris - Equipe Géophysique Spatiale et Planétaire, 4 Avenue de Neptune, 94107 Saint Maur des Fossés, France

ARTICLE INFO

ABSTRACT

This paper focuses on the shape of 31 shield volcanoes of small to intermediate size (a few tens of kilometers in diameter) in 5 regions of Mars: Tempe Terra, Syria Planum, Pavonis Mons, Arsia Mons and central Elysium Planitia. A model for the shape of these shield volcanoes is applied, based upon the concept of porous flow of an unconfined aquifer proposed by Lacey et al. [Lacey, A., Ockendon, J.R., Turcotte, D.L., 1981. On the geometrical form of volcanoes, Earth Planet. Sci. Lett., 54(1), 139–143] and developed by Turcotte and Schubert [Turcotte, D., Schubert, G., 2002. Geodynamics. Cambridge University Press, second edition]. The agreement between the topographic profiles and the theoretical shape suggests that the model is appropriate and can be used to derive the product of flow rate and viscosity ($Q\mu$). Estimates of $Q\mu$ are found to be homogeneous within a given volcanic region, but show large differences from one region to another, values generally decreasing with age (from oldest to youngest). Intrinsically, the method cannot separate the flow rate from the viscosity, but independent observations on individual lava flows in Syria Planum and central Elysium Planitia suggest that this evolution may be explained by decreasing magma viscosity with age. Independent constraints on the viscosity are used to interpret Q variations between volcanic regions. Except for Tempe Terra, and within error bars, relative effusion rates are essentially independent of volcano volumes, suggesting that the size of a shield volcano is principally controlled by the duration of volcanic activity. The specificity of central Elysium Planitia is emphasized, with highest flow rates associated with lowest lava viscosity. However, the lower viscosities at central Elysium Planitia cannot totally explain low $Q\mu$ values. Considering the equation of magma flow through a dike from a magma chamber at depth, to the shield, we suggest that lower volatile contents and/or deeper magma chambers may contribute to the decrease of $Q\mu$ values with time. Finally, the emplacement times of the 31 shield volcanoes were calculated using a calibration based upon terrestrial volcanoes Mauna Loa, Eldborgir, and Skjalbreiður. Emplacement times of martian volcanoes calculated in this way range from a few hundred thousand years (Tempe Terra) to a few tens of thousands of years (central Elysium Planitia). Despite the simplicity of the model, the quality of the fits and the internal consistency of the results are reasonable, encouraging development of more advanced models linking shield volcano shape to rheological properties of lavas and their characteristic time-scales of emplacement.

© 2009 Elsevier B.V. All rights reserved.

1. Introduction

Shield volcanoes commonly form on terrestrial and planetary surfaces. Examples on Earth include those in Iceland (Sigvaldason et al., 1992, Fig. 1), Hawaii (Hasenaka, 1994), Central Mexico and Idaho (Greeley, 1992). On Mars shield volcanoes range in diameter from a few tens of kilometers to hundreds of kilometers. Given that the topography of large volcanoes is potentially complicated by possible migration of the volcanic sources, deformation associated with flexure of the lithosphere and changes of eruptive style over time, we focus here on the topography of smaller features, a few tens of kilometers in diameter and a few hundred meters high. The Tharsis region on Mars contains many such structures, for example, those documented by Davis and Tanaka (1993) in Tempe Terra using Viking photoclinometric profiles, those on Syria Planum first recognized by Plescia and Saunders (1982) and characterized using Mars Orbiter Laser Altimeter (MOLA) and High Resolution Stereo Camera (HRSC) data by Baptista et al. (2008), or the numerous shield volcanoes and vents described south of Ascraeus Mons and Pavonis Mons, and within the caldera of Arsia Mons (Bleacher et al., 2007a). In addition to the Tharsis region, it is of note that 22 shield volcanoes have also been described in central Elysium Planitia (Tanaka et al., 2005; Vaucher et al., 2006, 2009, in revision) and these too are included in our analysis.

* Corresponding author.
E-mail address: david.baratoux@gmail.com (D. Baratoux).
[1] Now at CEPS/NASM MRC 315, Smithsonian Institution, Washington, D.C., 20013-7012, WA, USA.

Fig. 1. Top: Skjalbreiður volcano. Bottom: the Elborgir volcano (also named Lambahraun). These volcanoes are among the youngest on Earth. The Skjalbreiður volcano is at 1060 m high, and its crater is 300 m diameter. The diameter at the base is ~15–20 km. Eldborgir is 700 m high, and has a diameter of 10 km.

Shield volcanoes form primarily from successive lava flows erupted from the central vent, or from their flanks. Their growth is thus principally controlled by the flow parameters of the lava. The shape of such shields is distinct from cinder cones produced by ballistic fall of pyroclasts, the slopes of the latter being a function of the angles of repose of the volcanic and granular material (McGetchin et al., 1974; Calvari and Pinkerton, 2004). Martian shield volcanoes can be described by their diameter, height, aspect ratio, volume, and median slopes (Rossi, 1996; Hauber et al., 2009-this issue). These characteristics necessarily depend on primary factors, such as the rheological properties of the lava and effusion rates, and in principle it should be possible to extract rheological parameters from shield morphology. In practice, this requires well established models for volcanic construction, although numerous processes complicate this task, such as parasitic eruptions, explosive eruptions, landslides, and flank collapse. Models of volcano shape have nevertheless been proposed, such as that of Annen (2001) who took into account the relative contributions of magmatic intrusions and lava flows to volcano growth. However, many features of the model of Annen (2001) are the subject of debate, such as the spatial distribution of magma sources which is assumed to be uniform. An alternative model for the shape of shield volcanoes was proposed by Lacey et al. (1981) and developed by Turcotte and Schubert (2002). In Lacey et al. (1981), the flow of magma through the country rocks is compared to the flow of groundwater through an unconfined aquifer. Transport of magma to the surface is assumed to occur by porous flow through a pre-existing matrix made from previously emplaced and solidified lava flows, and in this case the surface of the volcano is equivalent to that of a phreatic surface of an unconfined aquifer.

Turcotte and Schubert (2002) argued that the model satisfactorily reproduces the shape of several terrestrial volcanoes, although previous work by Wadge and Francis (1982) and Wood (1982) had highlighted that (1) shield volcano shapes can be affected by ash falls, (2) the Dupuit approximation is not valid in the vent region, and (3) the theoretical shape does not reproduce the real shape of shield volcanoes. Concerning the first of these issues, martian shield volcanoes are likely formed almost exclusively from effusive eruptions. Indeed, there is no evidence of strong explosive activity associated with the emplacement of the shield volcanoes presented here, suggesting that the direct or indirect role of volatiles on volcano shape is limited (e.g. density changes of the melt phase or production of ash). Secondly, the Dupuit approximation requires slopes $dh/dx \ll 1$, which is the case for almost all of the topographic profiles presented here. Thirdly, we note that the shape of terrestrial volcanoes is complicated by plate motion, the migration of magmatic centers, and erosion by water, while the absence of plate tectonics and the relatively low erosion rates on Mars may make application of the model developed by Turcotte and Schubert (2002) more straightforward in that context. Finally, porous flow models have been successfully applied to model magma ascent (Scott and Stevenson, 1986), with specific applications to Mount Etna (Bonafede and Boschi, 1992; Bonafede and Cenni, 1998) and oceanic ridges (Angevine et al., 1984), providing further justification for exploration of the Turcotte and Schubert (2002) model.

With these elements in mind we begin by reviewing the mathematical derivation of shield volcano shape using the concepts described by Turcotte and Schubert (2002). We then compare the theoretical shape with 310 topographic profiles extracted from 31 shield volcanoes (10 for each volcano) from five regions of Mars. Estimates of the product of flow rate and viscosity for each volcano are then presented based upon the results of the model, along with an interpretation of the results in the different volcanic regions. Finally, a tentative estimate of the emplacement time of the martian volcanoes is proposed, based on comparison with terrestrial shield volcanoes for which the emplacement time may be independently constrained.

2. The shape of shield volcanoes

2.1. Mathematical derivation of shield volcano shape

We review here the calculation of the theoretical shape of shield volcanoes using the porous flow model of Lacey et al. (1981). In cylindrical coordinates, Darcy's law is:

$$u_r = \frac{k}{\mu}\frac{dp}{dr} \tag{1}$$

where u_r is the radial Darcy velocity (volumetric flow rate per unit area of the medium, which has the dimension of velocity), k is the permeability, and $p(r)$ is the pressure as a function of radial distance r. The topographic profile of the surface of the volcano is $h(r)$ and is analogous to the phreatic surface of the unconfined aquifer. For small slopes ($dh/dx \ll 1$), the Dupuit approximation is valid, and the radial Darcy's velocity is:

$$u_r = -\frac{k\rho g}{\mu}\frac{dh}{dr} \tag{2}$$

where ρ is the mass density of the fluid, g is the acceleration due to gravity at the surface, and μ is the dynamic viscosity of the fluid. This expression and those that follow do not apply to volcanic summits where steeper slopes invalidate the Dupuit approximation. In addition, because the summit may be strongly modified by caldera collapse, no attempt is made to model the topography of the summit region. As the volcano grows, mass conservation requires that:

$$\frac{\partial Q(r)}{\partial r} + 2\pi r\phi \frac{\partial h}{\partial r} = 0 \tag{3}$$

where ϕ is the porosity of the matrix and $Q(r)$ is the flow rate through a cylindrical surface of radius r and of height $h(r)$ given by:

$$Q(r) = 2\phi r h u_r = -\frac{2\pi k\rho g}{\mu}\left(rh\frac{\partial h}{\partial r}\right) \tag{4}$$

It is assumed that all the magma introduced to the central vent reaches the surface. Consequently, it is necessary to set $\phi = 1$ in the mass conservation equation. By substituting $Q(r)$ in Eq. (3), we obtain the Boussinesq equation in cylindrical coordinates valid in the limit of the Dupuit approximation:

$$\frac{\partial h}{\partial t} = \frac{k\rho g}{\mu r}\frac{\partial}{\partial r}\left(rh\frac{\partial h}{\partial r}\right) \tag{5}$$

This diffusion equation can be solved using the two similarity variables:

$$f = \left[\frac{k\rho g}{\mu Q_0}\right]^{1/2} h \tag{6}$$

and

$$\eta = \left[\frac{\mu}{k\rho g Q_0 t^2}\right]^{1/4} r \tag{7}$$

The Boussinesq equation can be transformed into a dimensionless form:

$$f\frac{d^2 f}{d\eta^2} + \left(\frac{df}{d\eta}\right)^2 + \frac{f}{\eta}\frac{df}{d\eta} + \frac{\eta}{2}\frac{df}{d\eta} = 0 \tag{8}$$

Assuming a constant volumetric flow rate of material injected at $r = 0$, the boundary condition is:

$$\lim_{r\to 0} -\frac{2\pi k\rho g}{\mu} rh\frac{\partial h}{\partial r} \to Q_0 \tag{9}$$

This boundary condition, expressed in terms of the similarity variables, can be written:

$$\eta f\frac{df}{d\eta} \to -\frac{1}{2\pi} \tag{10}$$

In addition to this boundary condition, there is a fluid flow front at $\eta = \eta_0$, while for $\eta > \eta_0$, $f = 0$. From Eq. (8), this condition can be rewritten as:

$$\left(\frac{df}{d\eta}\right)_{\eta = \eta_0} = \frac{1}{2}\eta_0 \tag{11}$$

2.2. Simulations of volcano growth

In this section we investigate the effects of the flow rate and viscosity parameters on the modeled volcano shape. Eq. (8) is solved numerically with the boundary conditions given by Eqs. (10) and (11) to obtain the general form $f(\eta)$ of shield volcanoes (see Appendix A). Volcanoes are simulated assuming martian gravity ($g = 3.71$), a permeability value of $k = 10^{-6}$ m^2 and a density of 2800 kg/m^3. The solutions are plotted for four combinations of viscosities (100 and 1000 Pa.s.) and flow rates (1×10^{-2} and 5×10^{-2} m^3/s) as a function of time (Fig. 2). Horizontal and vertical scales are identical to allow comparison. From Eq. (7), the volcano front may be described by:

$$r_0 = 1.16\left(\frac{k\rho g Q_0}{\mu}\right)^{1/4} t^{1/2} \tag{12}$$

The radius can be expressed as a function of the volume of the volcano, as $V = Q_0 t$, where t is the duration of the flow:

$$r_0 = 1.16\left(\frac{k\rho g}{Q\mu}\right)^{1/4} V^{1/2} \tag{13}$$

In general, viscosity affects the aspect ratio because flank slopes steepen with increasing viscosity. This model prediction can be assessed with the observed increase of flank slope with lava viscosity observed in Hawaiian shield volcanoes (Bleacher and Greeley, 2008). However, it is immediately seen from the equations that nothing can be said about viscosity and flow rate independently from volcano volume and diameter (or any other similar information describing the steepness of the volcano slopes). This could be a strong limitation of the model in the absence of independent data on lava viscosity or emplacement time. However, it is still possible to use this information to compare relative variations of the product $Q\mu$.

2.3. Influence of gravity on volcano shape

Several eruption parameters are influenced by the acceleration due to gravity, g, such as, the depth of the magma chamber, the pressure gradient driving magma ascent, and the flow rate of the lava (Wilson and Head, 1994). In the porous flow model, g appears in the numerator of Eq. (6). This implies that for a given value of $Q\mu$, the height of a volcano will be smaller on a planet with higher gravity, while its diameter will be larger. In detail, the height of the volcano depends on $g^{-1/2}$ and the radius on $g^{1/4}$ (Eq. (7)), satisfying mass conservation. This relation is independent of the maximum height of volcanoes, a parameter which scales with the thickness of the lithosphere, which is roughly inversely proportional to the radius of the planet and thus inversely proportional to gravity (Blasius and Cutts, 1976). Indeed, the model
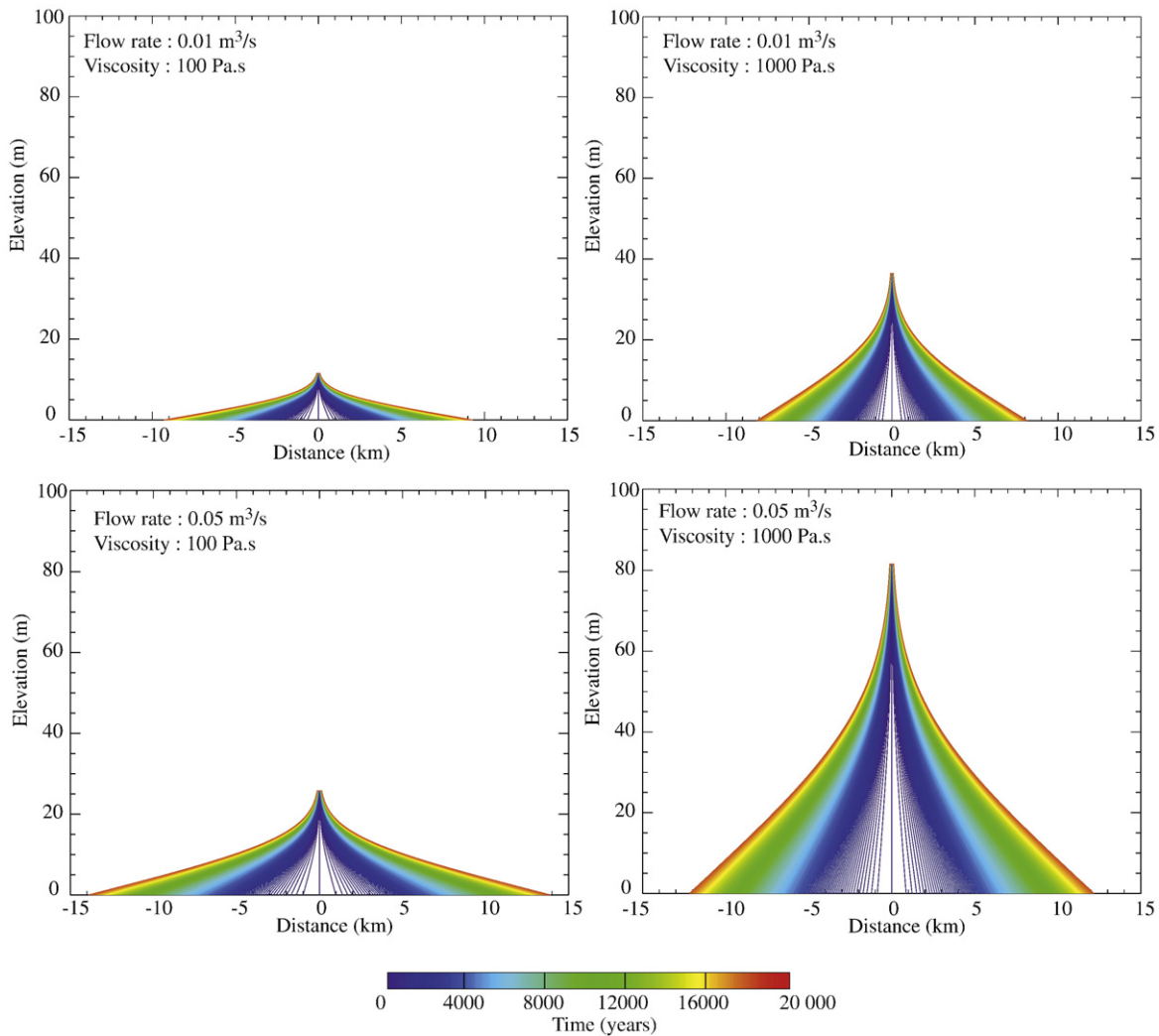
Fig. 2. Simulation of shield volcano growth according to the model of Lacey et al. (1981) and Turcotte and Schubert (2002). The simulations correspond to 4 combinations of μ (100 and 1000 Pa s.) and Q (1×10^{-2} and 5×10^{-2} m^3/s).

considered here only applies when the topography is significantly smaller than the maximum volcano height for a given planet (i.e., ≈ 30 km for Mars, ≈ 10 km for the Earth). This will be the case for the martian low shields considered in this paper.

2.4. Topographic profiles and adjustment method

In this section, we discuss the inverse problem and present our method to adjust the theoretical shape to observed topographic profiles. Topographic profiles were selected over each shield volcano and adjusted, using the least squares method, to the theoretical shape given by the numerical solution of Eq. (8). The origin of the x-axis is taken at one extremity of the profile, and the center of the volcano is considered as an unknown. An initial estimate of the location of the volcano center is given by visual inspection of the profile. A possible spatial domain for the center was also defined, and 30 equally spaced center locations were chosen within this domain. For each center location, the radial distance is converted to a non-dimensional radius. Two cases are considered here (Fig. 3): (a) it is assumed that the profile represents the entire volcano flank, and (b) it is assumed that the profile represents only a fraction of the volcano (i.e., part of the volcano is buried). In the first case, the distance to the center is divided by the maximum distance d_{max} to the center and multiplied by 1.16, as the base of the volcano occurs at a non-dimensional radius of 1.16. For
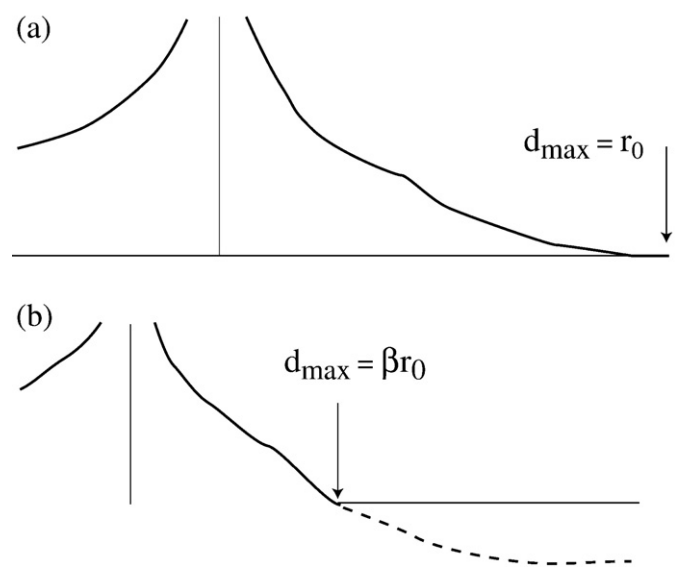

Fig. 3. Illustration of the adjustment methodology. Two cases are considered. In case (a), the flow front is exposed on at least one side of the topographic profile, and the maximum distance to the center of the volcano is equal to the volcano radius. For case (b), only a fraction β of the volcano is exposed, and the maximum distance to the center corresponds to βr_0 where r_0 is the radius of the volcano.

the second case, distances are converted to non-dimensional radii dividing them as in the previous case by the maximum distance d_{max} to the center and then multiplied by 30 different values ranging from 0.16 to 1.16. We define β as the proportion of the observed volcano such that $d_{max} = \beta \, r_0$. For case (b) 900 pairs of c and β values are considered and for each pair of values, a least squares minimization of the following function is performed:

$$F = \sum_{i=0}^{N} \left[\gamma h_i \left(\frac{1.16d}{2} \beta(x_i - c) \right) - f_i \left(\frac{d}{2} \beta(x_i - c) \right) \right]^2, \tag{14}$$

where f_i, η_i are sample points of the numerical solution of Eq. (8), h_i is the height of the volcano with respect to its base at non-dimensional radius η_i, N is the number of sample points, x_i is the distance along the topographic profile with the origin taken at the intersection of the volcano flank with the plain, and c is the location of the center of the volcano. γh_i is the non-dimensional height with γ corresponding to $(k\rho g/\mu Q)^{1/2}$ (Eq. (8)). The optimal values of γ are determined for each pair of c and β values and the associated value of F (the residuals) recorded. Cases where part of the volcano is not exposed ($\beta < 1$) correspond to burial of the volcano base by lava flows emanating from neighboring eruptions post-dating the formation of the studied shield. For these volcanoes, the real radius can be determined from the non-dimensional radius of 1.16 at the flow front and the value of γ. The thickness of the material covering the volcano base can be obtained from γ and the value of f at d_{max} corresponding to the contact with the emerged part of the volcano.

From the determination of the optimal value of γ, one may estimate the product of $Q\mu$. The optimal $Q\mu$ values were determined for all couples of c and β values. The residuals of each fit are also represented as a function of c and α. As suspected by Vaucher et al. (2009), the inverse problem for β is often poorly constrained. While it is generally possible to derive an optimal value of β corresponding to the lowest residual, this value is typically associated with a large error bar. Consequently, estimates of $Q\mu$ are given for both $\beta = 0$ and for the optimum value of β, or alternatively for a preferred value of β if the degree of embayment can be constrained from independent observations. In practice, as the shape of the volcano is never perfectly axisymmetric, several profiles are taken in various directions, and average values of γ and $Q\mu$ are computed with the associated standard deviations. The formal errors corresponding to individual least squares fits for each profile are used to estimate average values of γ and $Q\mu$. For instance, for the average value $<\gamma>$, we calculate:

$$< \gamma > = \sum_{j=1}^{N} \frac{\gamma_j}{\sigma_j^2 \sum_{i=1}^{N} \frac{1}{\sigma_i^2}} \tag{15}$$

where N is the number of profiles for a given volcano and σ_j is the error of γ_j associated with the fit of the profile j.

The inverse problem has three parameters, the center of the volcano c, the fraction of the volcano observed β and the quantity γ from which the value of $Q\mu$ can be derived. In order to test the robustness of the inverse problem for a partially buried edifice, and to determine to what degree the three parameters can be constrained, a synthetic volcano shape has been simulated using the values: $Q = 0.05$ m³/s, $t = 20,000$ years, $k = 10^{-6}$ m², $\mu = 100$ Pa s and $g = 3.7$ m s⁻². A fraction of the profile is extracted (indicated by the two arrows on Fig. 4), such that the exposed fraction of the simulated volcano is 60%. The simulated topographic profile is then used as the input data for the inversion procedure which consists in the determination of the optimal value of γ for each pair of β and c distributed over a 30×30 regular grid. The optimal value of $Q\mu$ corresponding to the global minimum of the residuals equals to 5.06 ± 0.20 J which is very satisfactory (the 1% offset from the initial value of 5.0 J results from the resolution of the grid for the parameters c and

β). We thus conclude that inversion of $Q\mu$ values from topographic profiles should not cause any difficulty. The residuals, as shown on the bottom of Fig. 4, indicate that the volcano center is also easily located from the inversion procedure. The correct value of $\beta = 0.6$ is also obtained, but associated with a broad minimum (Fig. 4). Considering accuracies from HRSC or MOLA topography on Mars, the fraction of the observed volcano will be thus difficult to constrain, even in the ideal case of a volcano that has not been affected by erosion. This limit is intrinsically due to the geometric properties of the theoretical shape. As a consequence, no attempt was made to give accurate estimates of β and we will limit the interpretation of our data to indicate whether a volcano is most likely to be entirely exposed or, alternatively whether a significant fraction is buried beneath the present-day surface.

3. Application to martian shield volcanoes

3.1. Geologic setting

The location of the shield volcanoes considered in this study is indicated on Fig. 5. In addition to Central Elysium Planitia, for the Tharsis region, volcanoes are grouped into four regions, Tempe Terra, Syria Planum, Pavonis Mons and Arsia Mons. Each volcano is labeled using three characters referring to the region (Tmp for Tempe Terra, Syr for Syria Planum, Pav for Pavonis Mons, Ars for Arsia Mons, and Cep for Central Elysium Planitia) followed by a character. The geographic coordinates of each volcano are given in Table 1. A brief geologic setting of each region is provided, in rough chronological order, from oldest to youngest. North of the Tharsis dome, shield volcanoes occur in Tempe Terra (Davis and Tanaka, 1993) dated as Hesperian (Moore, 2001; Skinner et al., 2006) that range in diameter from 10 km to 150 km. The volcanoes are aligned along north and north-eastern trending faults, and many volcanoes occur on grabens. The Syria Planum plateau covers >300,000 km and is centered at ~12°S, 256°E. It is bounded by faults such as Noctis Labyrinthus to the north, and Claritas Fossae to the west (Masson, 1980; Tanaka and Davis, 1988). The presence of shield volcanoes was first suspected from Viking images (Hodges and Moore, 1994) and confirmed by Baptista et al. (2008). Their diameters range from 10 to 30 km, with heights <200 meters; effusion rates estimated from individual lava flows are of the same order as Tharsis Montes (up to several thousand m³/s (Baptista et al., 2008)). The volcano-tectonic activity at Syria Planum was dated as Hesperian (3.5–3.7 Gy) by Baptista et al. (2008). This region is also characterized by a thick crust (80 km) possibly associated with a thin lithosphere at the time of magmatic activity, implying shallower sources of magma relative to the other sources that gave rise to the Tharsis Montes. Shield volcanoes were also mapped on caldera floors of Ascraeus Mons, Pavonis Mons and Arsia Mons (Bleacher et al., 2007b). These shields affect some terrains considered as young volcanic surfaces of Amazonian age (Skinner et al., 2006). A total of 95 low shields were identified, which are generally organized along a north-south direction. 22 shield volcanoes were documented in central Elysium Planitia (Vaucher et al., 2009, in revision) in the unit corresponding to the youngest lavas mapped by Tanaka et al. (2005) and Vaucher et al. (2006, in revision). Some of these shield volcanoes were dated at <100 Ma.

3.2. Comparison between topographic profiles and theoretical shapes

High-Resolution Stereo Camera (HRSC, Mars Express) and Mars Orbiter Laser Altimeter (MOLA, Mars Global Surveyor) Digital Elevation Models (DEM) were used in this study. For each volcano, we show one of the 10 profiles and the corresponding fit obtained from the method described in Section 2.4 (Figs. 6–9). For each volcano the location, volumes, and estimates of γ (in km⁻¹) are shown in Table 1 assuming that the volcanoes are entirely exposed ($\beta = 1$). In general, the fits are very good and residuals (root mean squares) are

generally <10 m, arguing for the validity of the model. In addition, results suggest that the effects of erosion are minimal even if some volcanoes are >3 Gy old. This idea is consistent with the fact that leveed lava flows a few tens of meters thick are observed on Syria Planum (Baptista et al., 2008).

In addition to these results, we have also explored the possibility that only a fraction β of the volcano is exposed, although, as discussed in Section 2.4, derived values of β will be associated with large error bars. Such analysis is also potentially useful to determine the relative chronology between shield volcanoes and the surrounding material. In general, two patterns are found when residuals are reported as a function of c and β. In most cases, the minimum residuals are found for $\beta = 1$ (i.e. the volcano is entirely exposed). In some other cases, the minimum values are found for low values of β (generally <0.1), while in a few cases, a broad minimum appears centered at a value of β ranging from 0.1 to 1 suggesting that the exposed fraction could be constrained for these volcanoes. In light of these results, the residuals associated with each profile and for each volcano are examined, and classified into four categories (Fig. 10):(1) residuals are minimum for $\beta = 1$, (2) residuals are minimum for undetermined values of β less

than 0.1, (3) residuals display a minimum for an intermediate value of β ranging from 0.1 to 1, and (4) the pattern of the residuals does not show any clear minimum and the situation is considered undetermined. The corresponding value of β is only shown in the third case. The percentage of profiles corresponding to each of the above categories is reported in Table 2. The average value (and standard deviation) of β is reported when several profiles fall into the third category. As the error bar on β is very large, the value of β should be considered with caution, even when the standard deviation obtained from several profiles is low. Table 2 shows that undetermined cases are rare and that the results for a given volcano are generally consistent among the profiles, with the exception of Syr7, Tmp3, Tmp4, Tmp5 and Pav1 for which slight discrepancies are reported. These discrepancies are generally limited to one or two profiles which may simply correspond to a local effect, not excluding the possibility that the base of the volcano is incorrectly identified given that the edges of profiles are selected from visual inspection of images and topographic data. In many cases, the volcano is entirely exposed and a fair proportion is confirmed by 100% of the topographic profiles for a given edifice. In particular, it is found that all the volcanoes in Syria
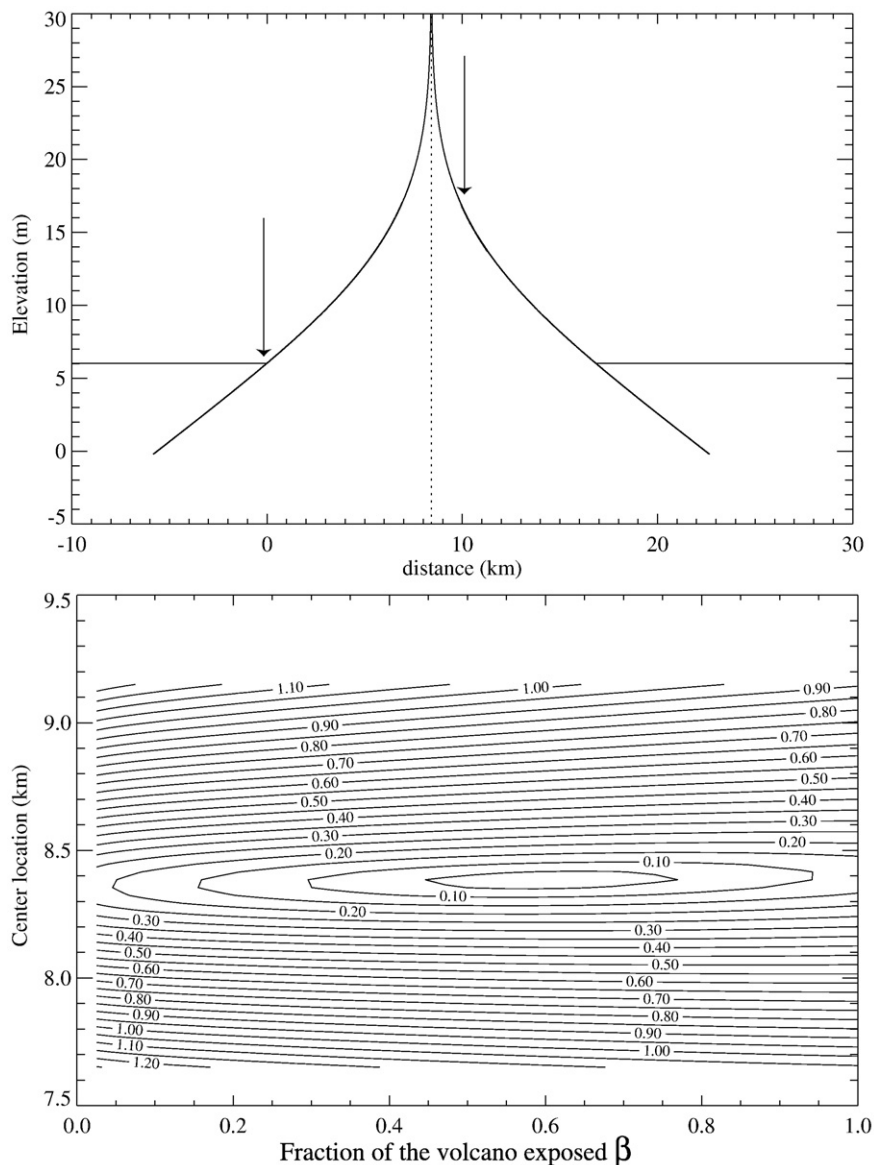

Fig. 4. Top: a simulated topographic profile of a shield volcano with $Q = 0.05$ m^3/s, $t = 20,000$ years, $k = 10^{-6}$ m^2, $\mu = 100$ Pa s and $g = 3.7$ m s^{-2}. Bottom: residuals of the fit as a function of c and β.
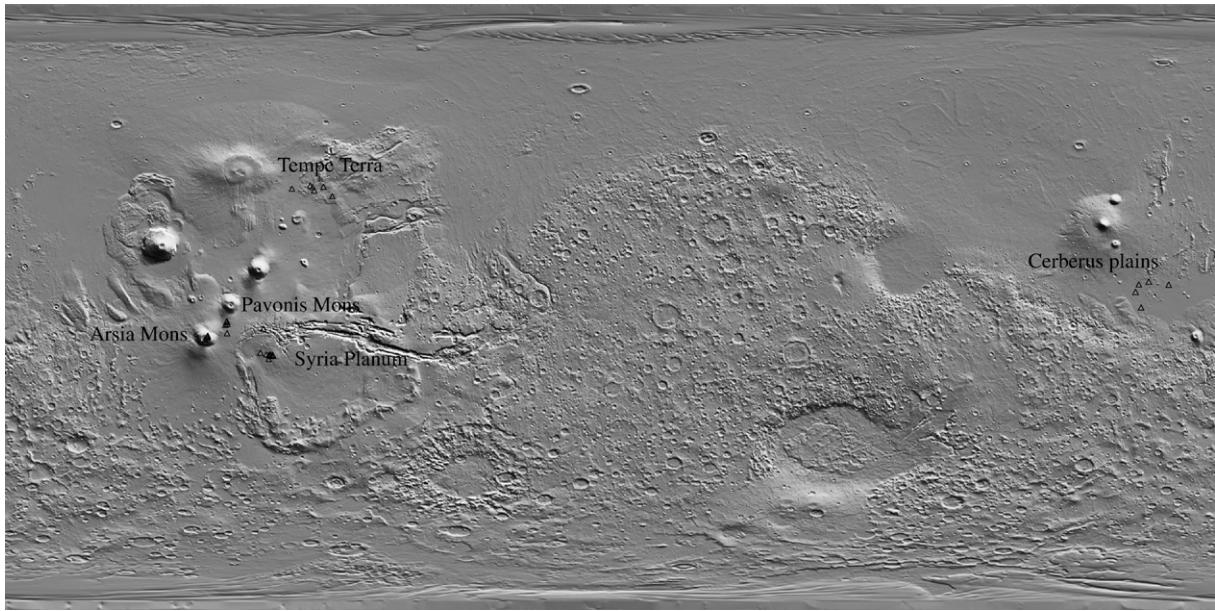
Fig. 5. Locations of the shield volcanoes studied: Tempe Terra, Syria Planum, Pavonis Mons, Arsia Mons and central Elysium Planitia.

Planum are entirely exposed, suggesting that they all postdate the terrain on which they formed. For the case of partial burial, the most spectacular case corresponds to the c volcano in central Elysium Planitia for which a relatively large thickness of lava cover is confirmed by 80% of the profiles. This interpretation was proposed by Vaucher et al. (2009) and confirmed from stratigraphic relationships determined with high resolution images of the contact between the volcano and the surrounding plain.

Table 1
Reference and coordinates of the shield volcanoes with volumes, areas, γ and $Q\mu$ estimates.

Reference	Longitude (°E)	Latitude (°)	Volume (km³)		Area (km²)		γ (km⁻¹)	$Q\mu$ (J)
			$V_{app/ext}$	V_{cor}	A_{app}	A_{cor}		
Tmp1	265.25	36	255	278	2771	3018	2.71 ± 0.25	1415 ± 265
Tmp2	274.8	36.6	181	280	2020	3059	2.65 ± 0.22	1475 ± 240
Tmp3	271.5	36.5	93	191	1563	2147	2.73 ± 0.19	1390 ± 190
(B)	271.5	36.5	1714	682		7650	1.98 ± 0.13	2655 ± 360
Tmp4	272	35.5	40	53	360	585	2.65 ± 0.14	1470 ± 160
(B)	272	35.5	478	190		2084	1.93 ± 0.11	2780 ± 310
Tmp5	277.4	33.7	11	16	173	222	9.37 ± 4.76	118 ± 120
Tmp6	270.8	37	126	169	1947	2294	3.44 ± 0.59	875 ± 300
SyrA	255.8	− 13.77	869	2402	8790	13335	1.48 ± 0.38	4717 ± 2400
Syr2	259.5	− 14.45	51	76	471	815	2.63 ± 0.38	1495 ± 430
Syr3	258.95	− 14.35	60	31	643	602	4.98 ± 1.13	418 ± 190
Syr4	258.42	− 14.36	41	48	573	657	3.34 ± 0.31	930 ± 170
Syr5	257.6	− 14.3	169	194	2247	1714	2.21 ± 0.30	2117 ± 580
Syr7	258.6	− 14.6	43	74	727	980	3.47 ± 0.59	860 ± 290
Syr8	259.17	− 14.71	46	52	720	711	3.72 ± 0.74	750 ± 300
Syr9	259.55	− 14.71	104	106	721	1101	2.54 ± 0.21	1600 ± 270
Syr12	258.33	− 15.68	46	78	661	1192	4.11 ± 1.16	613 ± 345
Pav1	245.77	− 7.83	83	74	1177	1190	3.90 ± 0.29	682 ± 101
Pav2	256.67	− 6.5	21	21	447	519	5.93 ± 0.40	295 ± 40
Pav3	245.3	− 5.26	27	37	692	918	5.93 ± 0.25	295 ± 25
Pav4	245.82	− 5.09	20	38	450	944	6.08 ± 0.71	280 ± 65
Pav5	245.58	− 4.4	10	21	425	597	7.02 ± 1.17	210 ± 70
Pav6	245.71	− 4.18	10	27	301	590	5.52 ± 0.65	340 ± 80
Ars1	239.16	− 9.65	21	12	506	422	9.10 ± 1.64	125 ± 45
(B)	239.16	− 9.65	113	44		1500	6.57 ± 1.10	240 ± 80
Ars2	239.75	− 9.41	46	102	1232	2080	4.91 ± 0.46	430 ± 80
Ars3	239.84	− 8.97	38	172	1090	2978	4.19 ± 0.25	590 ± 70
Ars4	239.91	− 8.8	10	110	586	1822	3.99 ± 0.21	650 ± 70
Ars5	239.94	− 8.6	17	95	629	1950	5.52 ± 0.65	340 ± 80
Cepa	160.63	− 0.01	148	208	3764	5518	6.44 ± 0.45	250 ± 35
Cepb	158.97	4.7	60	62	2089	3238	13.03 ± 1.39	61 ± 13
Cepc	159.95	6.93	214	264	6623	8646	8.60 ± 1.54	140 ± 50
(B)	159.95	6.93	2386	940		30800	6.25 ± 1.12	265 ± 95
Cepd	162.93	7.84	274	110	3793	3205	7.20 ± 0.76	200 ± 42
Cepe	168.94	6.88	119	261	6350	8256	9.49 ± 0.62	115 ± 15

Syr, Tmp, Cep, Pav and Ars refer respectively to Syria Planum, Tempe Terra, Pavonis Mons, Arsia Mons and central Elysium Planitia. (B) refers to estimates assuming that only a fraction of the volcano is observed ($\beta = 0.5$). See text for the definition of V_{app}, V_{ext}, V_{cor}, A_{app} and A_{cor}.

3.3. Surface area and volume of shield volcanoes

The first application of the porous flow model is to determine the volumes and surfaces of the shield volcanoes including potentially buried parts. When a volcanic edifice is entirely exposed, its area and volume can be estimated directly from topographic data. For its area, the contact of the base of the volcano with the surrounding plains is drawn as a polygon, and the area inside the polygon is estimated numerically. For its volume, a planar surface is optimized from points taken outside the volcanic edifice and the volume of the volcano is calculated by the difference between its topography and the planar surface. This operation was done using the gridview software provided by H. Frey at denali.gsfc.
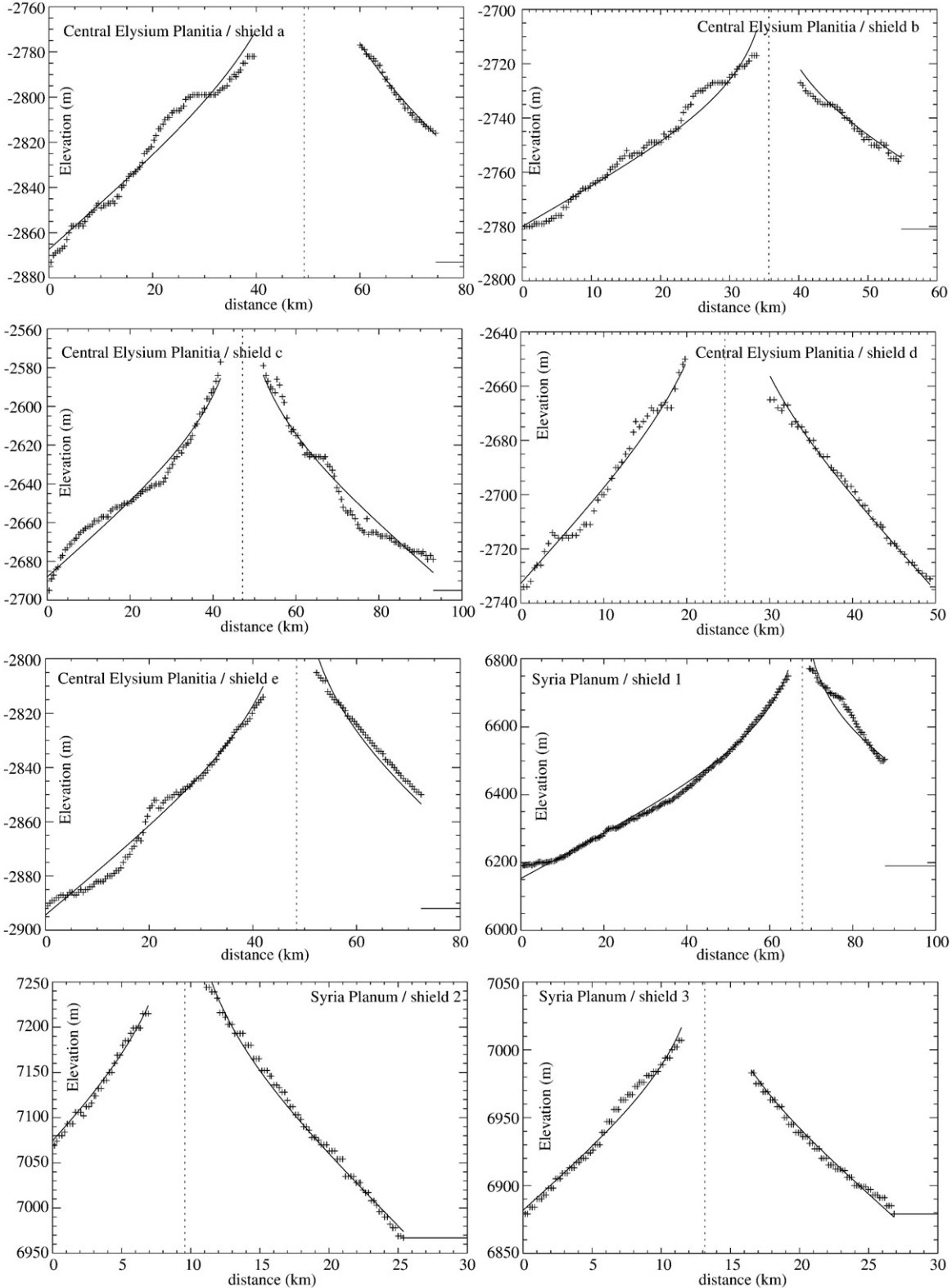
Fig. 6. Selection of topographic profiles and adjustments for shield volcanoes on Mars (part I).
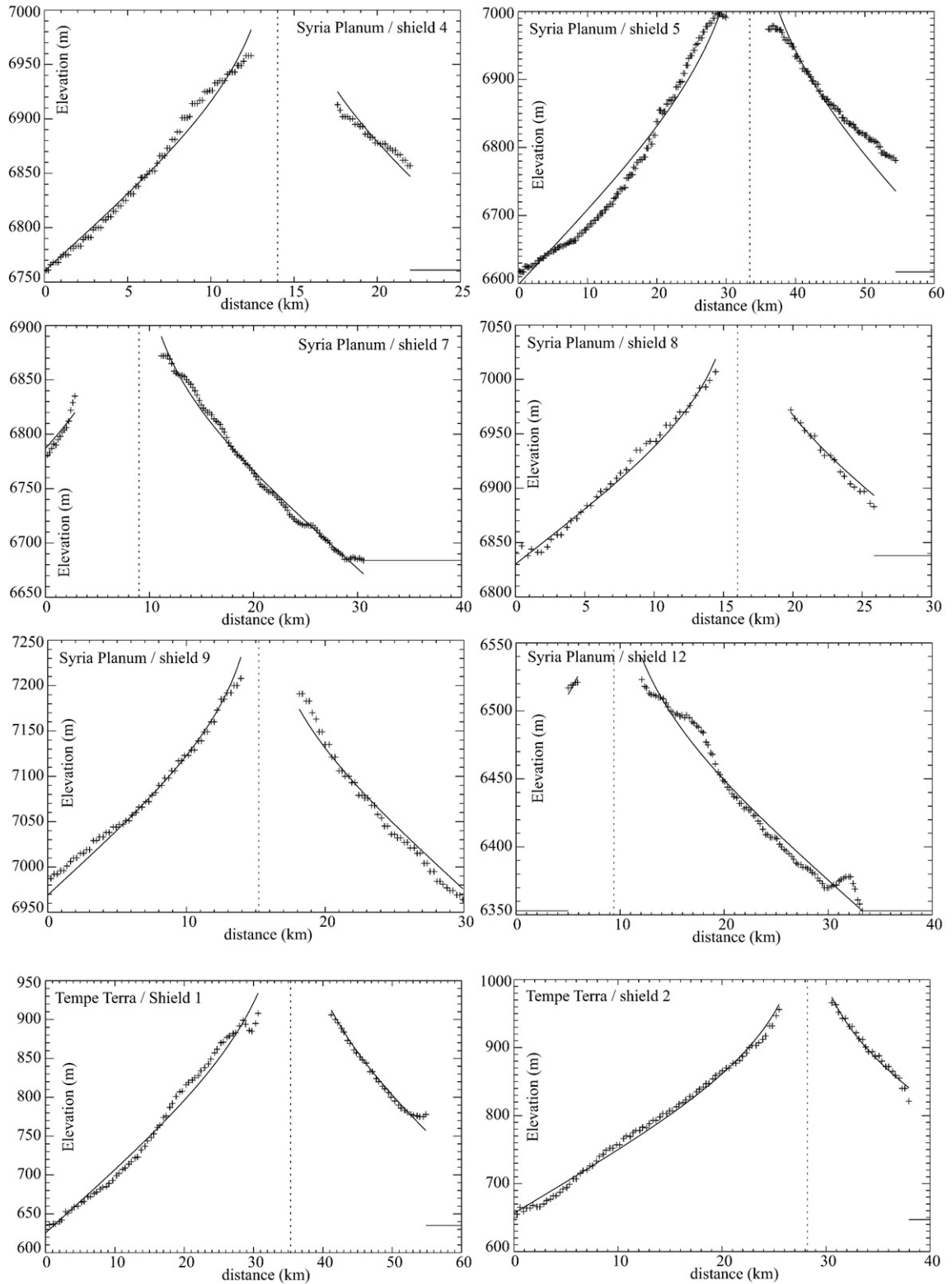
Fig. 7. Selection of topographic profiles and adjustments for shield volcanoes on Mars (part II).

nasa.gov/gridview. Apparent areas and volumes were estimated for all shield volcanoes (Table 1: V_{app} and A_{app}).

When part of the volcano is covered, the value of β is used to estimate the true area and volume of the volcano. The extrapolated area A_{ext} is given by:

$$A_{ext} = \pi \left(\frac{d_{max}}{\beta}\right)^2, \tag{16}$$

where d_{max} is the maximum radial distance averaged over the different profiles. The extrapolated volume V_{ext} may be written:

$$V_{ext} = V_{app} + \int_{d_{max}}^{d_{max}/\beta} 2\pi h(r) r \, dr + \left(\frac{d_{max}}{2}\right)^2 * z(r), \tag{17}$$

where $h(r)$ is the height of the volcano, and $z(r)$ is the thickness of material covering the base of the volcano. This expression can

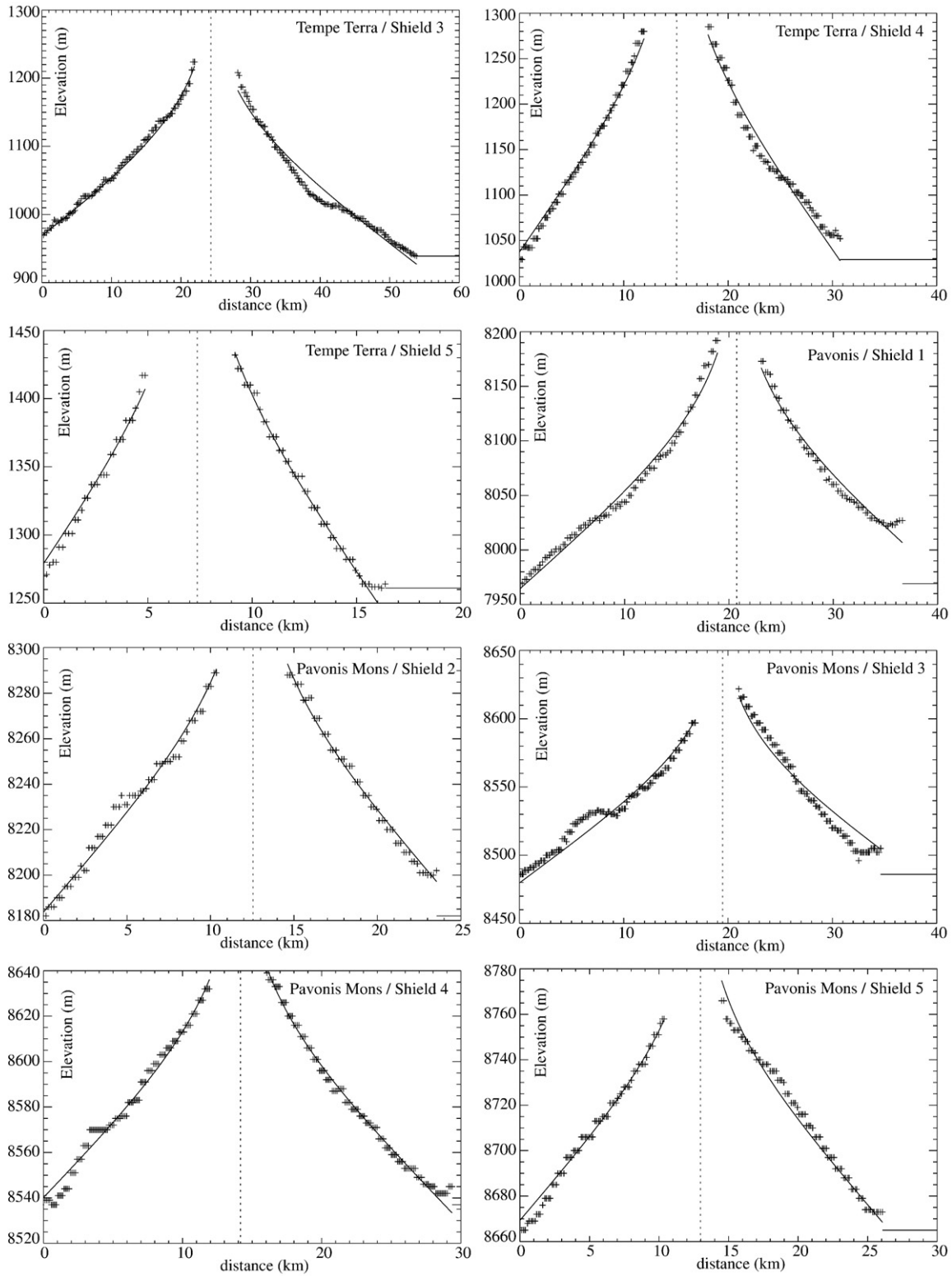**Fig. 8.** Selection of topographic profiles and adjustments for shield volcanoes on Mars (part III).

be written as a function of β, γ and non-dimensional heights and radii:

$$V_{\text{ext}} = V_{\text{app}} + \frac{2\pi}{\gamma}\left(\frac{d_{\max}}{1.16\beta}\right)^2 \int_{1.16\beta}^{1.16} \eta f(\eta)d\eta + \pi\left(\frac{d_{\max}}{2}\right)^2 \frac{f(\beta*1.16)}{\gamma}. \tag{18}$$

In this expression, the second term corresponds to the buried volume outside $d_{\max}$ and the third term corresponds to the buried volume between the center of the volcano and $d_{\max}$ considering the real elevation of the base of the volcano.

The topography of volcanoes was often influenced by obstacles, especially in the case of coalesced edifices, which are common in Syria Planum and Arsia Mons. In order to compare these volcanoes, it is useful

to normalize volumes and areas with a standard case defined as a fully developed and axisymmetrical shield volcano, using the porous flow model. For the volume, the theoretical shape can be integrated assuming axisymmetrical geometry as proposed above for the case $\beta < 1$. In this case, the integration is done for the entire volcano. As the fits are excellent in all cases, replacing the topographic profiles with the theoretical shape should have little consequence for the volume estimate. Following this approach, the total volume for both cases $\beta = 1$ or $\beta < 1$ is approximated by:

$$V_{cor} = \frac{2\pi}{\gamma} \left(\frac{d_{max}}{1.16\beta} \right)^2 \int_0^{1.16} \eta f(\eta) d\eta \approx 0.161 \frac{2\pi}{\gamma} \left(\frac{d_{max}}{1.16\beta} \right)^2 \quad (19)$$

Corrected areas (A_{cor}) are equal to extrapolated areas following the definition of A_{ext} in Eq. (16). When $\beta = 1$, the corrected area reduces to the area of a circle:

$$A_{cor} = \pi d_{max}^2 \quad (20)$$

For the non-buried cases ($\beta = 1$), apparent and corrected areas and volumes (Eqs. (20) and (19)) are shown in Table 1. For volcanoes where $\beta < 1$, a second line in Table 1 contains extrapolated and corrected volumes

(Eqs. (18) and (19)) and corrected areas (Eq. (16)). Where $\beta = 1$ the presence of obstacles whose areas were discarded for the apparent volume calculation explains why volume is systematically lower than that which would have fully developed in the case of a perfectly axisymmetrical shield. Corrected values are used systematically in the following, in particular when comparisons between volcanoes are discussed.

4. Discussion

The theoretical shape given by the porous flow model matches the shape of the small martian shield volcanoes, as shown above. We now discuss the physical meaning of the parameters k, μ and Q and suggest that the viscosity μ may be directly related to the viscosity of the lava. The interpretation of the flow rate is then discussed using independent estimates of viscosity, before calculating the emplacement times of the martian shield volcanoes, based on a calibration using terrestrial volcanoes.

4.1. Flow rate × viscosity as a function of volume

$Q\mu$ values derived from the fits of the topographic profiles linearly depend on the permeability value chosen to represent the solidified matrix through which the magma ascends. Permeabilities of basalt are
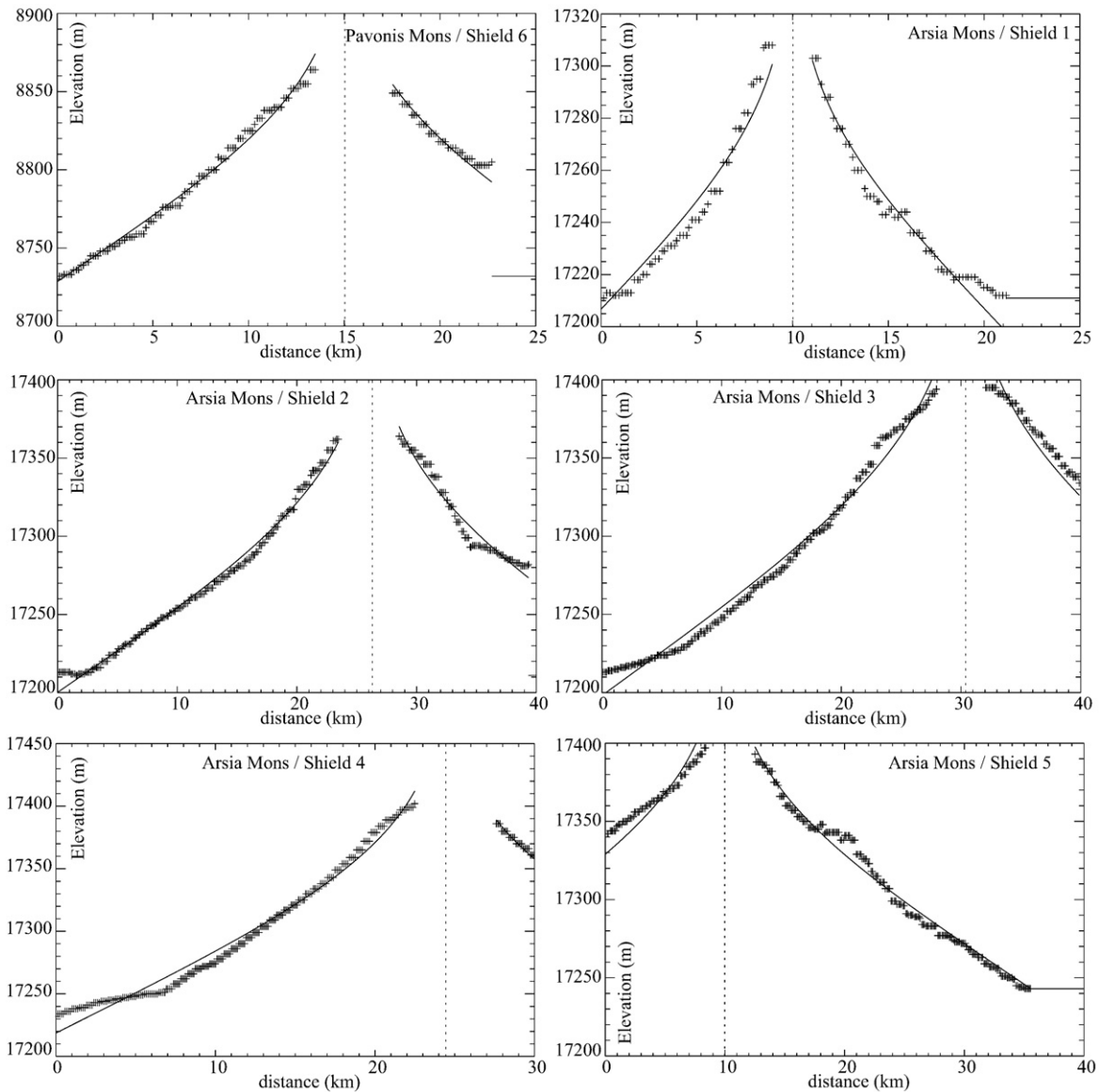

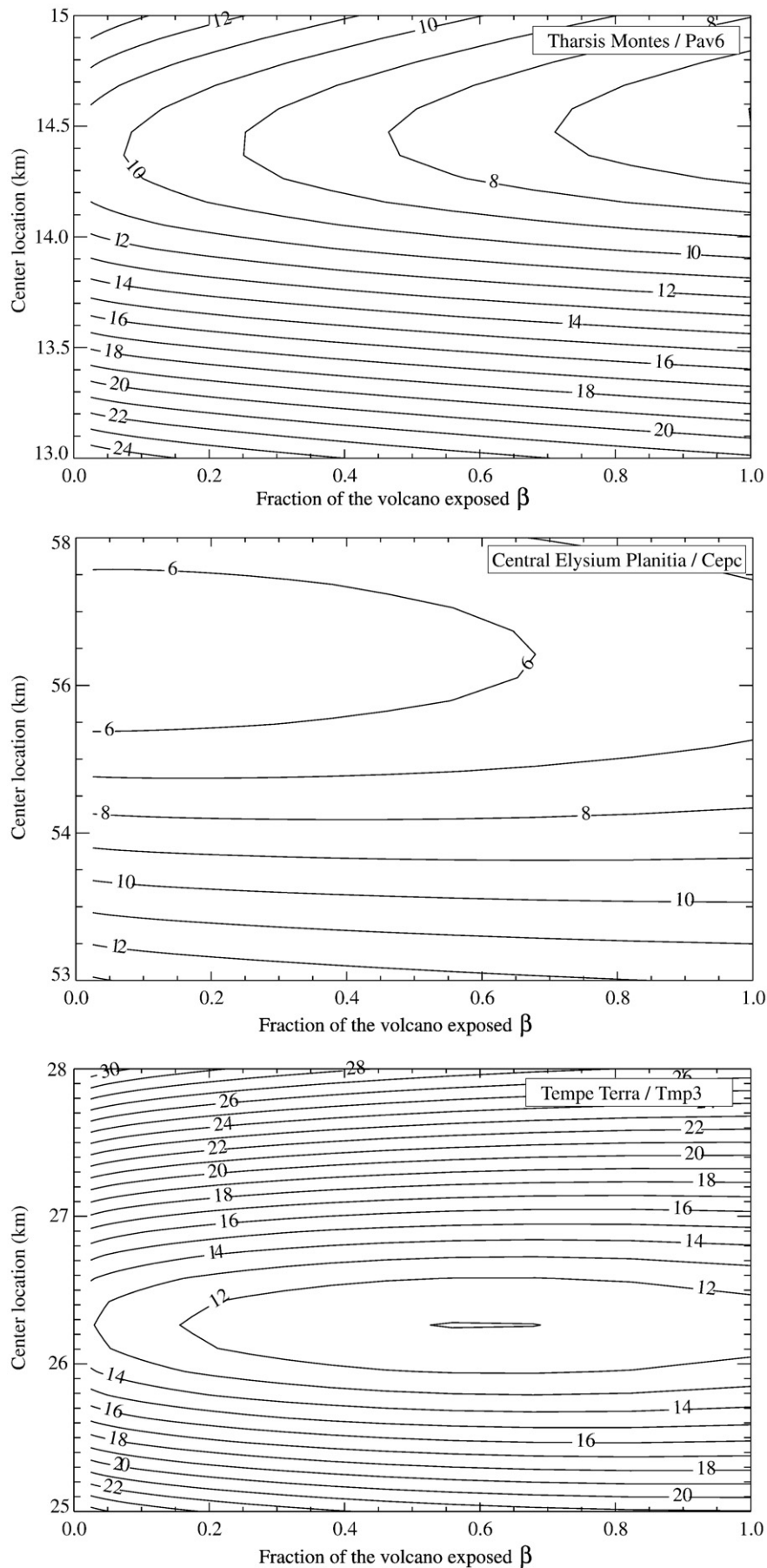**Fig. 9.** Selection of topographic profiles and adjustments for shield volcanoes on Mars (part IV).

Fig. 10. Illustration of 3 of the 4 possible cases for the residuals patterns as a function of volcano center and β (the fraction of the volcano observed) Top: the lowest values of the residuals are found for $\beta = 1$. Middle: the lowest values of the residuals occur for low and undetermined β values (<0.1). Bottom: a broad minimum occurs for an intermediate value of β ranging from 0 to 1.

Table 2
Table of the exposed fraction of each shield volcano. Syr, Tmp, Cep, Pav and Ars refer respectively to Syria Planum, Tempe Terra, Pavonis Mons, Arsia Mons and central Elysium Planitia.

Reference	Entirely observed	Partially observed			Undetermined
		$\beta<0.1$	$0.1<\beta<1.0$	β	
Tmp1	80%	–	–	–	20%
Tmp2	80%		10%	0.35 ± 0.2	10%
Tmp3	10%	20%	70%	0.3 ± 0.2	–
Tmp4	30%	40%	20%	0.2 ± 0.1	10%
Tmp5	70%	20%	–	–	10%
Tmp6	10%	40%	50%	0.5 ± 0.2	–
SyrA	30%	0%	20%	0.7 ± 0.2	50%
Syr2	100%	–	–	–	–
Syr3	90%	–	–	–	10%
Syr4	80%	–	–	–	20%
Syr5	100%	–	–	–	–
Syr7	65%	20%	–	–	15%
Syr8	100%	–	–	–	–
Syr9	90%	–	–	–	10%
Syr12	90%	–	–	–	10%
Pav1	10%	10%	60%	0.1 ± 0.1	20%
Pav2	70%	–	30%	0.5 ± 0.2	–
Pav3	80%	–	20%	0.5 ± 0.2	–
Pav4	100%	–			–
Pav5	100%	–			–
Pav6	100%	–			–
Ars1	–	100%	–	–	–
Ars2	40%	10%	40%	0.7 ± 0.1	10%
Ars3	60%	–	20%	0.8 ± 0.1	20%
Ars4	–	–	100%	0.7 ± 0.2	–
Ars5	100%	–			–
Cera	60%	–	–	–	40%
Cerb	20%	–	–	–	80%
Cerc	–	80%	–	–	20%
Cerd	100%	–	–	–	–
Cere	100%	–	–	–	–

For each volcano a series of ten profiles has been extracted. The fraction of profiles falling into one of the 4 following categories is reported: (1) the profile reaches, at least for one side, the contact of the flow front with the surrounding terrain, (2) a fraction of the volcano lesser than 10% is observed, (3) a minimum is observed for $0.1<\beta<1.0$. In this case, the value of this minimum and the standard deviations when several profiles confirm this situation are reported, (4) no clear minimum for the residuals.

known to vary by several orders of magnitude and the absence of permeability measurements for the studied shield volcanoes is unfortunate. However, we note that the relevant permeability most likely concerns the ascent of magma through fractures and voids such as lava tubes, etc. First of all, this will lead to effective permeabilities much higher than those of "compact" basalt rock samples which have permeabilities typically about 10^{-11} m^2. Secondly, the fact that lava will pass through fractured rock should act to reduce the variation in permeability relative to that expected for compact samples. We thus propose that the effective permeability is constant, with a relatively high value of 10^{-6} m^2. This value is consistent with a medium having pores several centimeters in size, considered to approximate typical voids found in fresh basaltic lava flows. This choice directly affects calculated values of $Q\mu$, and it should thus be kept in mind that absolute values of $Q\mu$ may potentially be shifted to lower values. With a value of permeability of 10^{-6} m^2, estimates of $Q\mu$ range from 10^3 J to 10^5 J (Table 1). $Q\mu$ estimates are calculated first assuming that the base of the volcano is exposed. However, according to the results presented in the Table 2, volcanoes Tmp3, Tmp4, Cepc, Ars1 are most likely partly covered. Estimates of $Q\mu$ are thus also given for these volcanoes considering the case $\beta<1$. As an accurate determination of β values is not possible, we have arbitrarily chosen an intermediate value of 0.5 for the volcanoes Tmp3, Tmp4, Cerc, and Ars1.

While estimates of $Q\mu$ range from a few hundred to a few thousand Joules, they are relatively constant within a given volcanic region, suggesting that similarities of the physical characteristics of the magma source are revealed by this approach, including the dimension, depth,

and chemical composition of the magma. On the other hand, differences from one region to another are observed. Volcanoes having similar volumes but different $Q\mu$ estimates by several orders of magnitude suggest differences in lava viscosity and/or effusion rates. In order to extend investigation of the origins of the differences between volcanic regions, the products $Q\mu$ are represented as a function of corrected volcano volume (Fig. 11) as explained in Section 3.3. This figure clearly shows two important features. First of all, $Q\mu$ values are, to a first approximation, correlated with volcano volumes. These trends can be fitted using a power law for each region. In regions where one or more volcanoes are partly buried, two lines are given, assuming no or partial burial. For the case of no burial, the following expressions describe the data, where V is the volume expressed in km^3:

$$Q\mu_{\text{Tempe}} = 741 \pm 190 \times V^{0.12 \pm 0.05} \tag{21}$$

$$Q\mu_{\text{Syria}} = 116 \pm 62 \times V^{0.52 \pm 0.11} \tag{22}$$

$$Q\mu_{\text{Pavonis}} = 33 \pm 18 \times V^{0.64 \pm 0.15} \tag{23}$$

$$Q\mu_{\text{Arsia}} = 38.9 \pm 25.9 \times V^{0.55 \pm 0.14} \tag{24}$$

$$Q\mu_{\text{Cep}} = 11.6 \pm 8.1 \times V^{0.50 \pm 0.13} \tag{25}$$

Taking account of the idea that only 50% of the volcanoes Tmp3, Tmp4, Ars1 and Cepc are exposed, the expressions for these three regions become:

$$Q\mu_{\text{Tempe}} = 473 \pm 116 \times V^{0.26 \pm 0.04} \tag{26}$$

$$Q\mu_{\text{Arsia}} = 55.5 \pm 60.5 \times V^{0.47 \pm 0.23} \tag{27}$$

$$Q\mu_{\text{Cep}} = 7.45 \pm 6.5 \times V^{0.58 \pm 0.17} \tag{28}$$

These trends are represented by solid lines for non-buried cases and dotted lines for buried cases in Fig. 11. The coefficients of the power laws highlight the differences among regions. The exponents associated with volumes are generally ~0.5, except for the case of Tempe Terra, which is four times lower. This coefficient increases when the values for buried volcanoes (Tmp3 and Temp4) are corrected leading to an average value of 0.5 ± 0.14. In a rough chronological order from the oldest to the youngest, $Q\mu$ values are relatively high for Tempe Terra, intermediate for Syria, lower for Pavonis and Arsia Mons, and lowest for central Elysium Planitia. It is remarkable that $Q\mu$ estimates appear to decrease with the age of the volcanic regions. Differences in $Q\mu$ values between Tempe Terra and central Elysium Planitia are about two orders of magnitude. As the method cannot separate the effusion rate from the viscosity, it is not immediately clear which of these parameters controls the variations in the product $Q\mu$, although this point will be discussed in more detail below.

4.2. Relative effusion rates as a function of volume

The meaning of effusion rate in volcanic settings has been clarified by Harris et al. (2007), and is briefly summarized here. The *instantaneous effusion rate* is defined as the volume flux of erupted lava that is feeding a flow at any particular point in time. *Time averaged discharge rates* consider volume fluxes averaged over a period of time. *Eruption rate* is defined as the total volume of the lava emplaced since the beginning of the eruption divided by the time since the eruption began. *Mean output rate* is the final volume of erupted lava divided by the total duration of the eruption. As a consequence of these definitions, *instantaneous effusion rate*, *time-averaged discharge rate*, *eruption rate*, and *mean output*
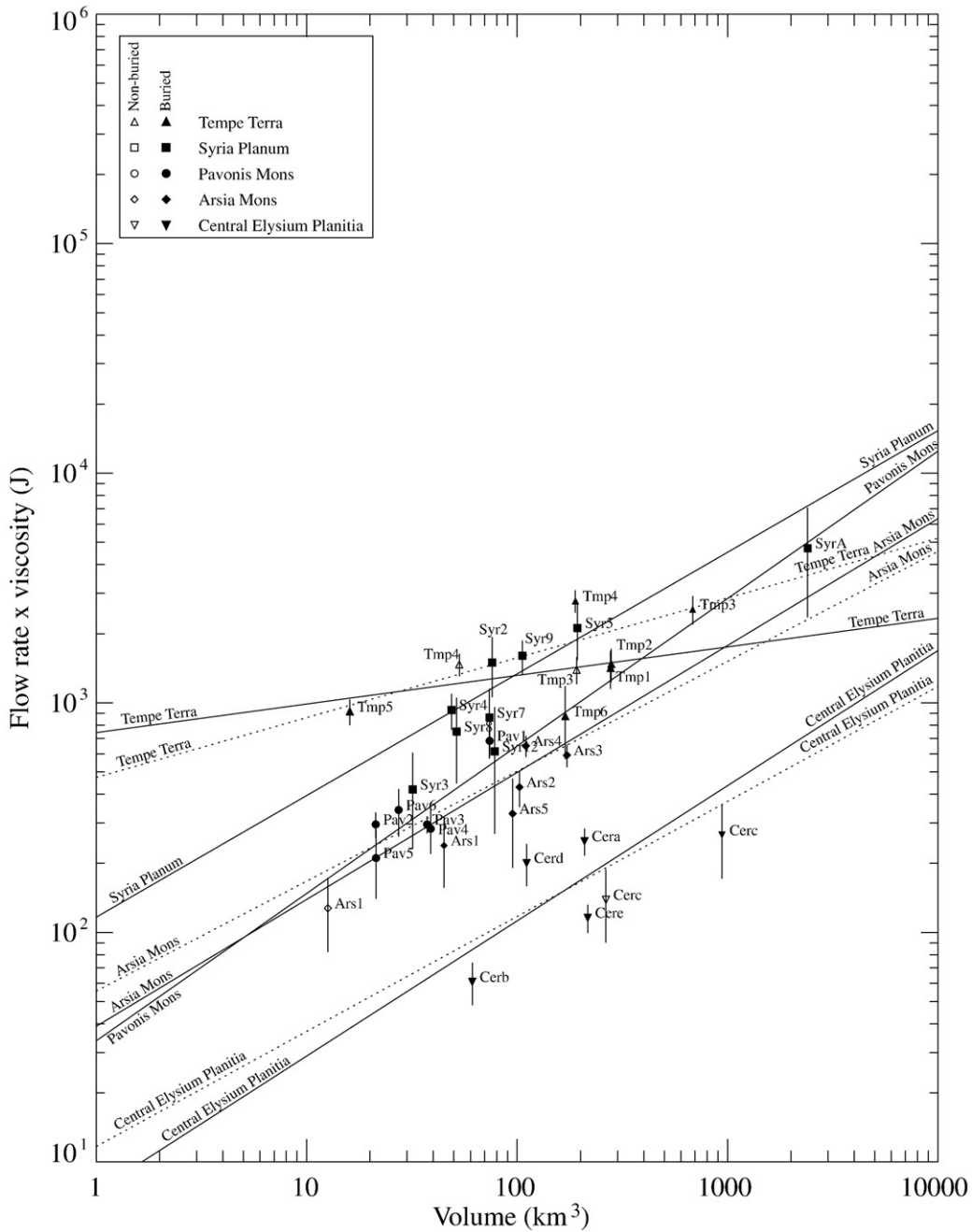
Fig. 11. Viscosity × flow rate products as a function of volumes for martian volcanoes.

rate consider volumes emplaced over increasing periods of time. In addition to the temporal definitions, it is then necessary to define the spatial scale at which these definitions are relevant, from that of a single flow to that of a regional scale. The total volume flux feeding all units across the entire compound flow field will give the *total effusion rate* for all active units. Following these definitions, the volumetric flow rate considered in the unconfined aquifer model would correspond to the total effusion rate if all the surface of the shield volcano were active during an eruption, which is not the case. There is thus no direct equivalence between the flow rate involved in the aquifer model and any definition of effusion rates. Consequently, we will continue to use the term *flow rate* to refer to the parameter Q involved in the porous flow model, while the term *effusion rate* (q) will be used only when referring to lava eruption. A way to reconcile the effusion rate q with the shape-derived flow rate Q would be to normalize the former by the total area of the volcano, and the latter by

the total active area composed of all surface flows for one eruptive event:

$$q = Q \times \frac{a}{A}, \tag{29}$$

where q is the average total effusion rate for a single eruption, A is the area of the volcano, and a is the active area (or the area affected by the single eruption). The relevant average value for the ratio a/A is unknown and absolute effusion rates cannot be derived from this model. However, it is possible to compare the results using $Q\mu$ estimates normalized by the areas of each volcano (Fig. 12). When presented in this way, the correlation with the volcano volume is no longer apparent. Consequently, larger volcanoes may essentially result from eruptions of longer duration rather than from higher average total effusion rates for individual eruptions. As observed previously, a

general decrease of the area-normalized $Q\mu$ values is observed as a function of the ages of the volcanic regions.

Taking the interpretation one step further, it is possible to compare normalized effusion rates if independent values of viscosities are available. Viscosity is a constant during growth in the porous flow model, but is known to vary during lava emplacement and cooling in association with crystal growth. However, considering that the equilibrium surface is achieved during the flow of the lava within the edifice before it cools, the relevant value for the viscosity parameter should be the viscosity at magmatic emplacement temperatures. Independent measurements of the rheology of lava flows exist only for the shields in Syria Planum and central Elysium Planitia. In central Elysium Planitia, lava flows were shown to be extremely fluid (less

than 1000 Pa s following Jaeger et al. (2007) and Vaucher et al. (2009)), which is also qualitatively suggested by the particularly low slopes of the shield volcanoes. Following Baptista et al. (2008) and Vaucher et al. (2009), values of 10^6 Pa s. were found for Syria and adopted for all martian volcanoes, except for those of central Elysium Planitia for which a viscosity of 10^3 Pa s was considered. It should be kept in mind that regional differences may be related to these choices of viscosity values and the consequences of alternative choices should be discussed. Relative effusion rates (ER) were thus obtained from $Q\mu$ values divided by volcano areas and the viscosity values indicated above. ER values given in Fig. 13 as a function of volumes are also normalized by the average of ER values including all volcanoes. We note here that ER values are independent of the choice of the
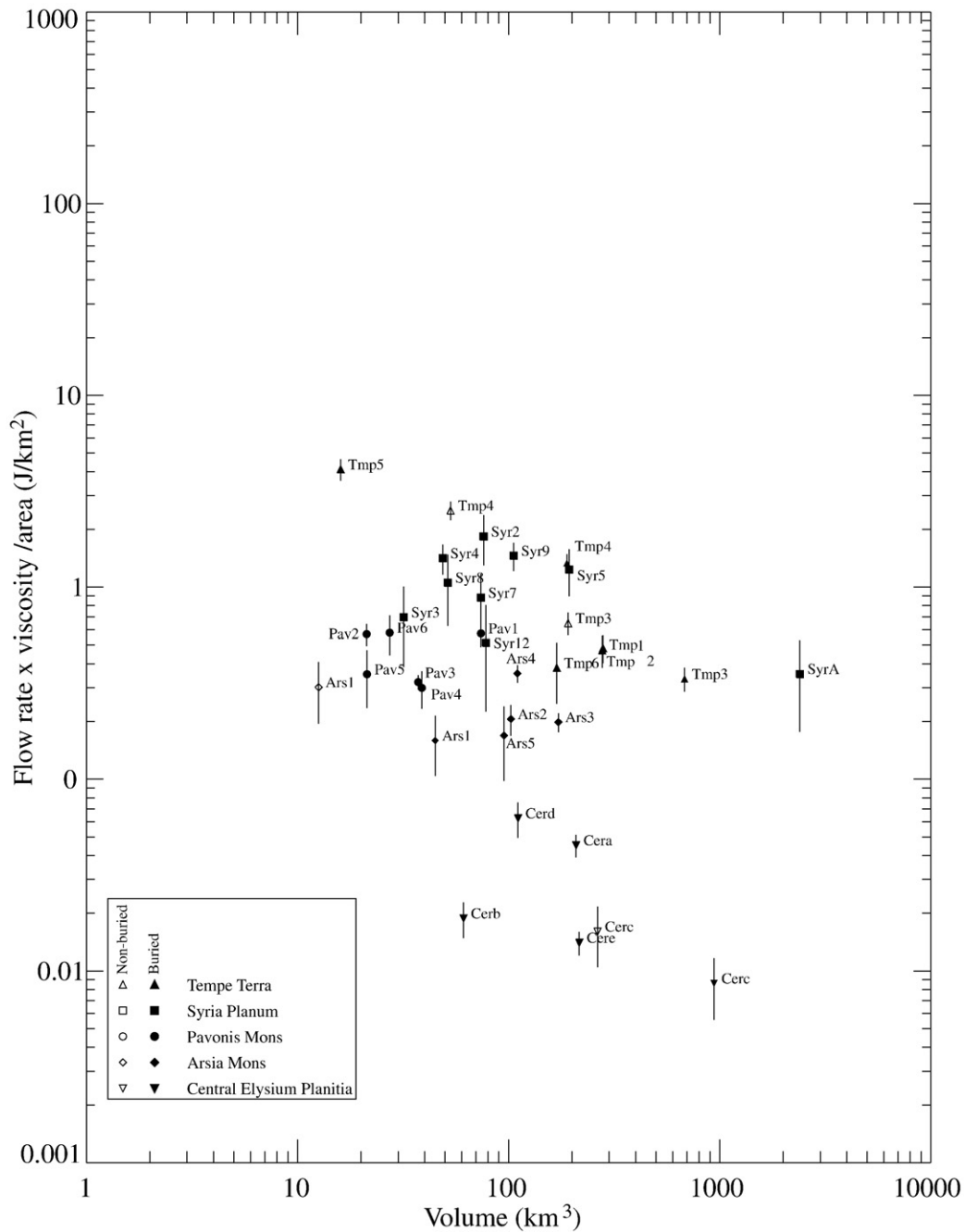

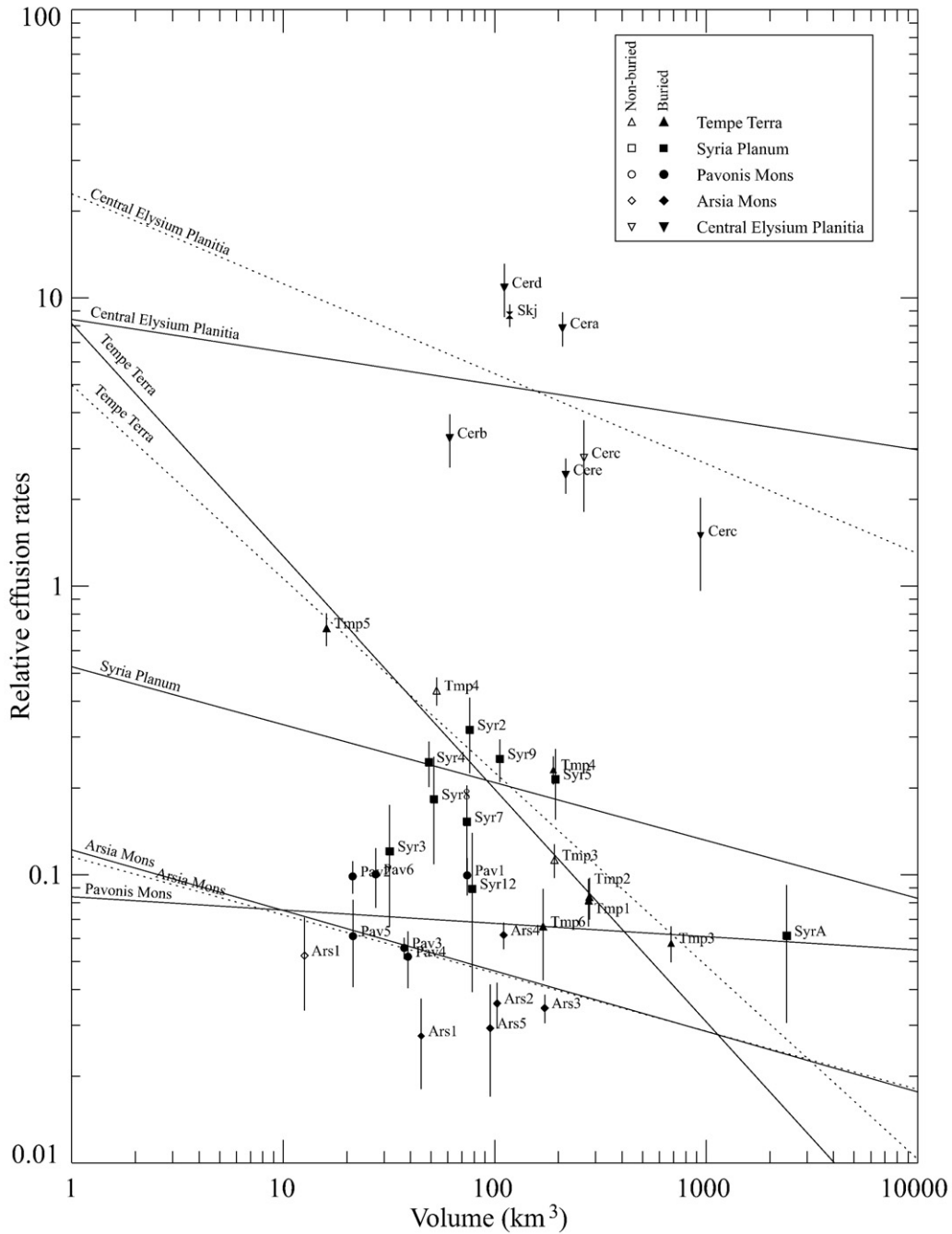Fig. 12. Viscosity × flow rate products normalized by the area of the volcano as a function of volumes.

Fig. 13. Relative effusion rates as a function of volumes. Flow rates (Q) are obtained from independent estimates of viscosity (10^6 Pa s for martian volcanes, except for those of Central Elysium Planitia for which a value of 10^3 Pa s has been chosen). Then effusion rates are obtained by dividing Q by the volcanoes areas and values are finally normalized using the average of all values.

permeability value. This dependence between ER and volume can be quantified by power-law relationships:

$$ER_{\text{Tempe}} = 8.15 \pm 2.07 \times V^{-0.81 \pm 0.06} \tag{30}$$

$$ER_{\text{Syria}} = 0.52 \pm 0.28 \times V^{-0.20 \pm 0.12} \tag{31}$$

$$ER_{\text{Pavonis}} = 0.08 \pm 0.04 \times V^{-0.05 \pm 0.15} \tag{32}$$

$$ER_{\text{Arsia}} = 0.12 \pm 0.08 \times V^{-0.21 \pm 0.13} \tag{33}$$

$$ER_{\text{Cep}} = 8.42 \pm 7.34 \times V^{-0.11 \pm 0.17} \tag{34}$$

Considering that the volcanoes Tmp3, Tmp4, Ars1 and Cepc are partly exposed (50%), the above equations become:

$$ER_{\text{Tempe}} = 4.97 \pm 1.23 \times V^{-0.67 \pm 0.05} \tag{35}$$

$$ER_{\text{Arsia}} = 0.11 \pm 0.13 \times V^{-0.20 \pm 0.22} \tag{36}$$

$$ER_{\text{Cep}} = 23 \pm 16 \times V^{-0.31 \pm 0.13} \tag{37}$$

Except for Tempe Terra, the relative effusion rates are, within error, essentially independent of volume (exponent values are close to zero). Among the values obtained, central Elysium Planitia displays

the highest effusion rates. This result depends on the independent viscosity estimates on Syria Planum and central Elysium Planitia from individual lava flows using the Jeffrey's equation. As mentioned in Vaucher et al. (2009) and Baptista et al. (2008) the absolute values of viscosity could be offset as this equation has not been calibrated for the martian environment. However, the relative variations of viscosity between the Syria and the central Elysium Planitia volcanoes should be real. Thus, we are confident in the relative differences in effusion rates between these two regions. The cases of the other volcanic regions cannot be addressed with confidence as we do not have independent values of viscosity. It is thus not possible to conclude with confidence about the evolution of effusion rate with time. Furthermore, it is of note that effusion rates and viscosities should be related, following the expression of Wilson and Head (2002):

$$Q = \frac{W^2 L P}{8 \mu d} \tag{38}$$

where W and L are the vent width and length, respectively, P is the pressure driving the ascent of the magma, and d is the depth of the roof of the magma reservoir. Thus, variations of $Q\mu$ with time may reflect variations of L, P, or d rather than independent variations of viscosity and effusion rates. In particular, the lower values of $Q\mu$ for central Elysium Planitia, resulting from lower viscosities by three orders of magnitude should be compensated by effusion rates three orders of magnitude higher. However, this is not the case, as effusion rates are only one order of magnitude higher. Estimating the average dimensions of volcanic vents for the different regions is difficult because the vents are often eroded and partly cover by lavas. Systematic changes with time of vent dimensions have never been suggested and seem unlikely. A lower pressure in magma chambers at central Elysium Planitia due, for instance, to lower volatile contents of the magma, can contribute to the decrease with time of $Q\mu$

values. This hypothesis is consistent with the idea that the present martian mantle is likely depleted in volatile elements. Alternatively, a volatile-poor magma of higher density or a lower density of the crust may be responsible for the formation of magmatic chambers at larger depths Wilson and Head (1994). Following this idea, variations of $Q\mu$ values may be also controlled by magma chamber depths.

4.3. Emplacement time

Results from the model can be used to constrain the emplacement times for each volcano. It is not possible to obtain the emplacement times for the volcanoes directly from flow rates and volumes, as the proportion of time during which each volcano is active and the average active area for each eruption are unknown. Nevertheless, the emplacement time of the volcano can be written:

$$T = \frac{V}{qp} = \frac{VA}{Qpa} \propto \varepsilon \frac{VA}{Q} \tag{39}$$

where p is the average proportion of time during which the volcano is active and ε is a factor equal to the unknown product pa. With the objective to compare emplacement times, we assume that the parameter ε is constant and the same on Mars and on Earth. With this assumption, it is possible to calibrate the unknown parameters in Eq. (39) from a known emplacement time of a terrestrial volcano. Suitable terrestrial shields for the application of the Turcotte and Schubert (2002) model have thus been assessed for this purpose.

4.3.1. Calibration from terrestrial shield volcanoes
Terrestrial volcanoes suitable for this application should meet several requirements: (1) volcanoes built entirely from effusive eruptions should be targeted, such that no modification of the shape
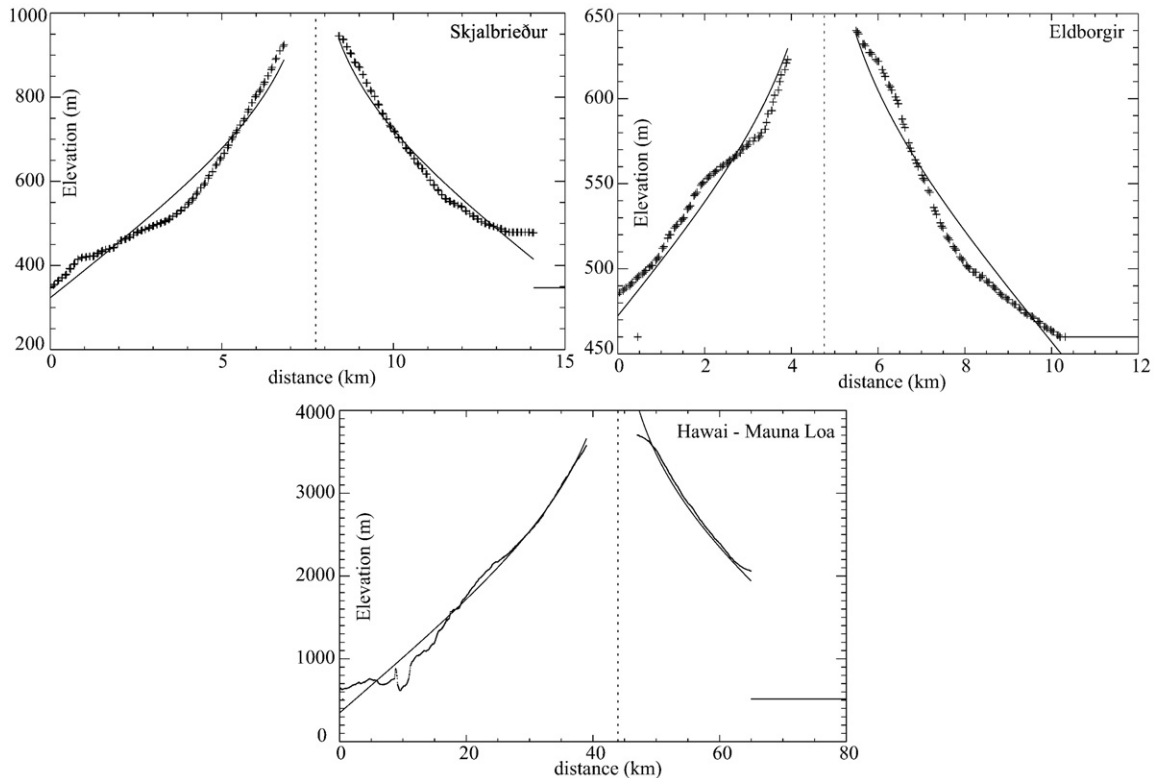

Fig. 14. Three selected topographic profiles of the Skjalbreiður, the Eldborgir (crosses) and the Mauna Loa (dots) and the result of the adjustment on the theoretical shape (plain line).

Table 3
Reference, coordinates, volumes and estimates of the flow rate × viscosity products for terrestrial shield volcanoes.

Volcano name	Ref.	Volume (km³)		Area (km²)		γ (km⁻¹)	$Q\mu$ (J)
		$V_{app/ext}$	V_{cor}	A_{app}	A_{cor}		
Eldborgir	Eld	20.74	6.33	150	111	4.24 ± 0.28	1530 ± 200
(B)	Eld	41	10.5		184	3.71 ± 0.25	2000 ± 275
Skjalbreiður	Skj	60.7	33	180	174	1.27 ± 0.06	16900 ± 1600
(B)	Skj	296	118		622	0.94 ± 0.04	31260 ± 2800
Mauna Loa	Mau	12170	7056	5000	7970	0.28 ± 0.04	350 000 ± 91000

(B) refers to estimates assuming that only a fraction of the volcano is observed ($\beta = 0.5$ for the Skjalbreiður and $\beta = 0.8$ for the Eldborgir). See text for the definition of $V_{app/ext}$, V_{con}, A_{app} and A_{cor}.

has resulted from intermittent explosive activity, (2) the volcanic event should be young enough that the original shape of the volcano has not been significantly affected by erosion, and (3) as the model assumes constant viscosity during the emplacement of the shield, volcanoes showing a significant evolution of the magma composition should be avoided as this affects the physical characteristics of the lava (e.g., variations of viscosity related to the silica content of the lava). Best candidate volcanoes are the well known Icelandic shields, Skjalbreiður and Eldborgir. In order to apply the model on a larger volcano, we also chose the Mauna Loa in Hawaii, even if the longer history of the latter, the effects of erosion, the flexure of the lithosphere and the evolution of magma composition (Bleacher and Greeley, 2008) make it less suitable for this application. As the island of Hawaii is composed of 5 volcanoes (Kohala, Mauna Kea, Huala-lai, Mauna Loa, Kilauea), we have extracted topographic profiles for the lava surface belonging to the major volcano, Mauna Loa, using the map given in Garcia et al. (2007).

SRTM data (resolution 3″ per pixel for Iceland, 1″ per pixel for Hawaii) were used to extract 10 topographic profiles for each volcano. The fit was achieved by assuming that each profile reaches the flow fronts at least on one side (case a, Fig. 3). Three selected profiles for
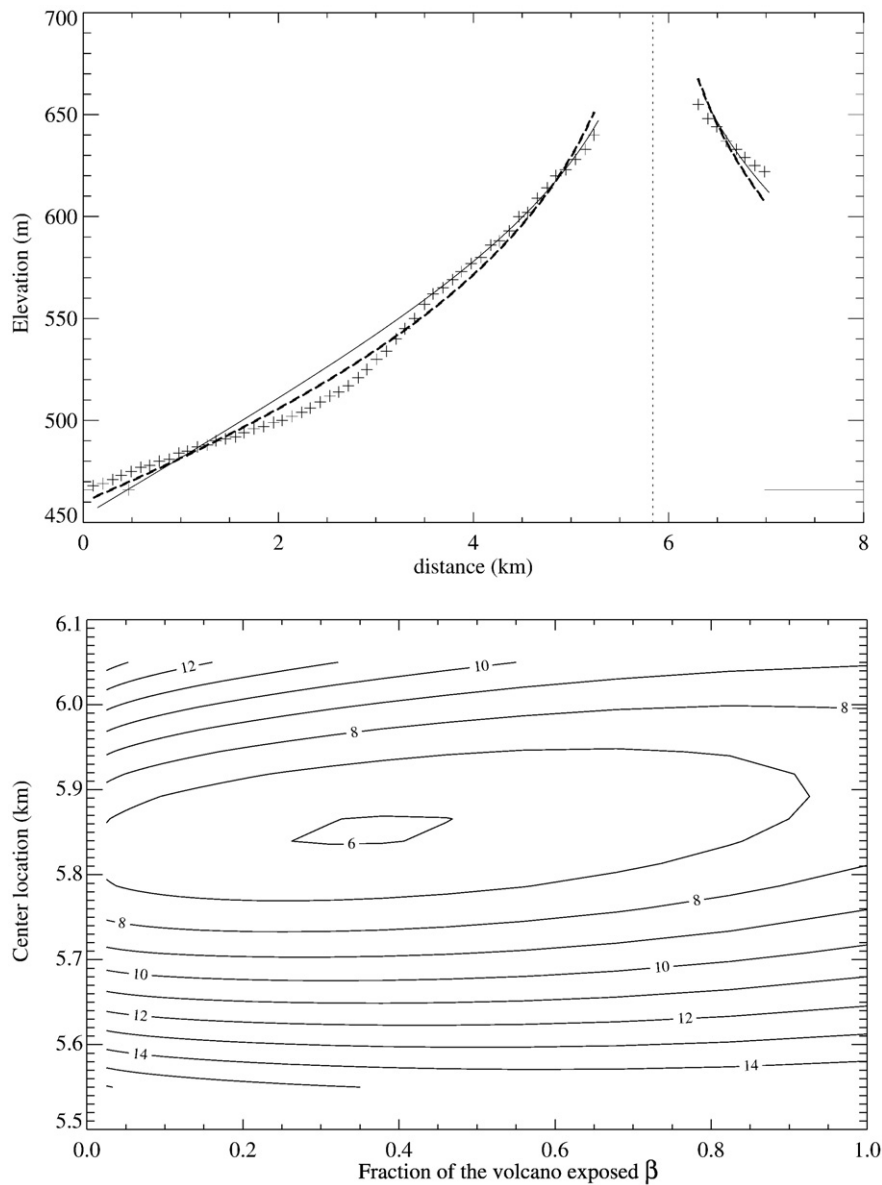

Fig. 15. Top: a topographic profile of the Eldborgir (crosses) and two adjustments. The plain line corresponds to the assumption that the topographic profile extends to the flow fronts, and the dotted lines result from an adjustment assuming that only a fraction of the shield can be observed. Bottom: residuals of the adjustments as a function of the position of the center of the volcano and of the fraction of the volcano which is sampled in the topographic profile. While the pattern suggests that only a part of the volcano is observed, the shape of the minimum is too broad to constrain quantitatively the real diameter of the volcano.

each of the volcanoes are shown on Fig. 14. Estimates of the $Q\mu/k$ and γ values averaged for the 10 profiles are given in Table 3. As for the martian shield, a permeability value of 10^{-6} m^2 is chosen for the estimates of $Q\mu$. Adjustments were also made assuming that volcanoes are partly buried (case b, Fig. 3).

For Eldborgir, the adjustment is slightly better when one considers that a part of the volcano is buried (Fig. 15) with residuals <10 m. Eldborgir lava flows were mapped by Sinton et al. (2005) revealing the difficulty in obtaining a complete topographic profile that would correspond to the theoretical shape. To the north, it is likely that part of the lava flows are covered by an ice sheet, and have been partly eroded by the advance and retreat of the glacier (Baratoux et al., 2005). To the south, the emplacement of the lava was strongly controlled by the rough pre-existing topography of eroded hyaloclastite ridges and the flow of the lava was driven toward the southwest. Given that we believe that a relatively large fraction of the Eldborgir is likely exposed, a corresponding β value of 0.8 was chosen.

Skjalbreiður is older than Eldborgir and is partly covered by more recent lavas (Sinton et al., 2005), and is also more eroded. Geochemical data led Sinton et al. (2005) to distinguish two episodes, suggesting different chemical and physical characteristics of the magma. This complexity may partly explain higher (but acceptable) residuals ranging from 10 to 20 m. The representation of the residuals as a function of the center of the volcano and of the fraction of the volcano exposed suggests that a relatively small fraction of the volcano is actually observed. As illustrated in Fig. 16, the minimum residuals of all the profiles suggest a value of β<0.6, but as explained before, it is difficult to give an accurate estimate of this fraction. The thickness of material covering the base of the volcano should not exceed the local elevation (~300 m), and a corresponding minimum value of 0.5 was selected.

For Mauna Loa (Fig. 17), it is found for all profiles that it is not necessary to invoke a buried fraction of the volcano. Minimum residuals are generally <100 m per point. The base of the volcano is taken as the contact with the sea, although the shield extends to the ocean floor, ~5000 m below sea level. However, we a priori consider only the subaerial part for the fit because the topography of the submarine part of the Mauna Loa is controlled by different processes than in the subaerial environment. At depth, water pressure maintains effusive eruptions, and basalt is emplaced as pillow lavas. At shallower depth, the contact between the hot lavas and the water can become explosive and results in the formation of hyaloclastites. In Hawaii, hyaloclastites are found down to 900 m deep, overlying the pillow lavas (Garcia et al., 2007). The accumulation of hyaloclastites formed a plateau with steep slopes on which effusive volcanism took place from the time eruptions started to occur above sea level. The fact that the theoretical shape applies directly to the emerged part of the volcano is consistent with this scenario of formation. In addition, the quality of the fit indicates that we are not able to detect the signal due to the deformation associated with the flexure of the lithosphere for a volcano of this size.

The most robust estimate of the emplacement time is given for Mauna Loa which is on the order of magnitude of 1 million years (Clague and Dalrymple, 1987), while time scales on the order of magnitude of hundreds/thousand of years are proposed for the Iceland shields (Sinton et al., 2005). The emplacement time is thus calibrated using the Mauna Loa emplacement time T_{ML} for all other volcanoes:

$$T = \frac{VA}{Q} \frac{(Q\mu)_{ML}}{V_{ML}A_{ML}} \frac{T_{ML}}{\mu_{ML}} \tag{40}$$

where the subscript ML refers to the values for Mauna Loa. Estimates of emplacement times for martian volcanoes thus depend on the inverse of the viscosity value adopted for the Mauna Loa. It should be noted first that if the same value of viscosity for the Mauna Loa and the Iceland shields is used, the emplacement time for the Icelandic shields is on the order of thousands of years, in good agreement with the maximum emplacement times bounded by the ages of these volcanoes (~9000 years for Skjalbreiður and ~3000 years for Eldborgir, (Sinton et al., 2005)). Viscosities ranging from 10^2 to 10^6 Pa s have been suggested for lava flows in Hawaii (Table 4 Hiesinger et al., 2007; Harris and Allen, 2008). Viscosity values obtained by direct measurements on terrestrial lava flows may differ by one order of magnitude with viscosity derived on the martian surface from the Jeffrey's equation. This level of uncertainty led us to use the same viscosity between terrestrial shields and all martian shields, inferred to be composed of basalts, with the exception of those of central Elysium Planitia which were more fluid. Using this calibration, the calculated emplacement times for the martian
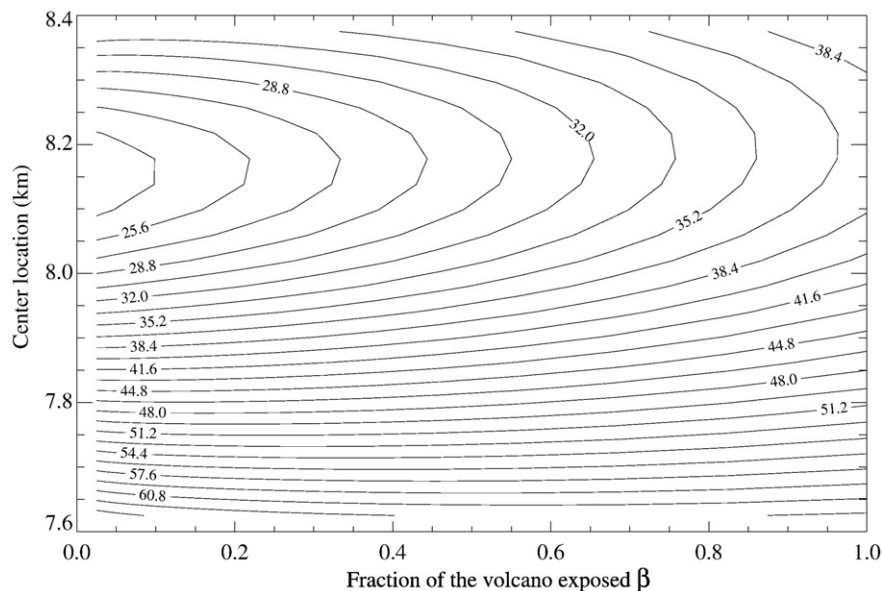

Fig. 16. Residuals as a function of the position of the center of the volcano and of the fraction of the volcano for the Skjalbreiður volcano. The shape of the minimum suggests that a small fraction of the diameter of this volcano is observed, and that it is partly covered by more recent lavas.
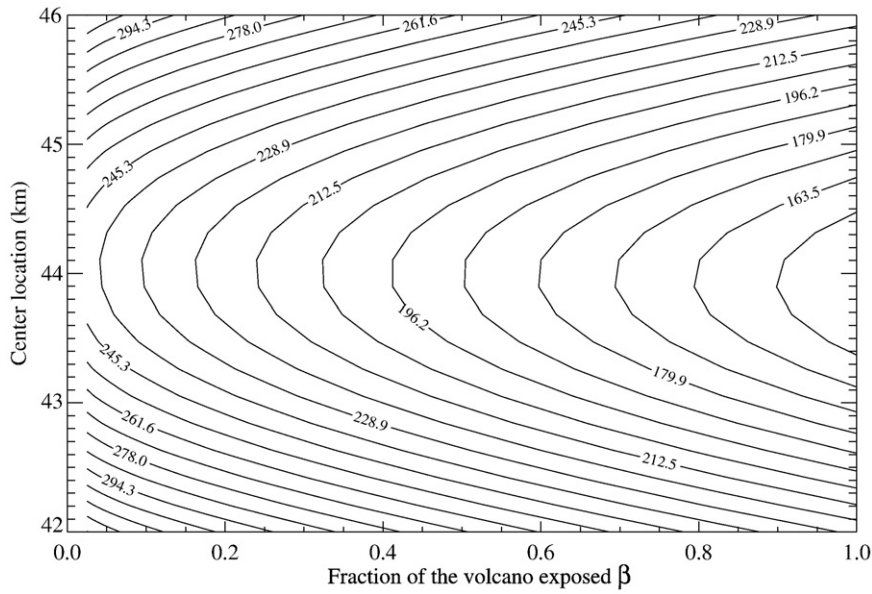
Fig. 17. Residuals as a function of the position of the center of the volcano and of the fraction of the volcano for the Mauna Loa volcano. The shape of the minimum suggests, conversely to the previous cases, that the volcano is entirely observed.

volcanoes as a function of volume are shown in Fig. 18. This approach demonstrates that the emplacement time increases with the size of the volcano, as expected if average effusion rates are independent of volumes. As for the other representations of the results, power-laws between emplacement times and volumes can be derived:

$$Etime_{Tempe} = 131 \pm 33 \times V^{1.80 \pm 0.05} \qquad (41)$$

$$Etime_{Syria} = 2040 \pm 1097 \times V^{1.20 \pm 0.11} \qquad (42)$$

$$Etime_{Pavonis} = 12815 \pm 6935 \times V^{1.04 \pm 0.15} \qquad (43)$$

$$Etime_{Arsia} = 8813 \pm 5872 \times V^{1.20 \pm 0.13} \qquad (44)$$

$$Etime_{Cep} = 127 \pm 111 \times V^{1.11 \pm 0.17} \qquad (45)$$

When it is considered that 50% of the volcanoes Tmp3,Tmp4, Ars1, and Cepc is exposed, the expressions become:

$$Etime_{Tempe} = 440 \pm 110 \times V^{1.40 \pm 0.04} \qquad (46)$$

$$Etime_{Arsia} = 636 \pm 693 \times V^{1.74 \pm 0.22} \qquad (47)$$

$$Etime_{Cep} = 209 \pm 144 \times V^{1.00 \pm 0.13} \qquad (48)$$

The emplacement times are expected to vary proportionally with the volume if effusion rates are constant, which is generally the case (exponents are close to 1), with the exception of Tempe Terra, for which the exponent is closer to unity when corrected values for the embayed Tmp3 and Tmp4 volcanoes are considered. An opposite situation is found for the region of Arsia Mons region, suggesting that the value β = 50% for Ars1 might not be appropriate. It should also be noted that Cepc is closer to the average trend for this region when burial is taken into account. Emplacement times for all the volcanic regions, with the exception of central Elysium Planitia, range from several hundred thousands of years to a few million years. For central Elysium Planitia shields, emplacement times as low as a few tens of thousand of years are found. This approach is a unique way to discuss the emplacement time of the small martian shield volcanoes because crater counting methods cannot be applied for this purpose. The results at central Elysium Planitia emphasize the unique nature of this regional volcanic activity.

5. Conclusion

In this paper, the theoretical shape for shield volcanoes proposed by Lacey et al. (1981) and Turcotte and Schubert (2002) was applied to 31 martian shield volcanoes from 5 regions. Low residuals suggest that the similarity of the shapes of all small shield volcanoes on Mars can be explained in the context of the model. In addition, results suggest that the topography of the 31 shield volcanoes studied in this paper were only slightly affected by erosion since their formation. Surprisingly, this result is equally valid for both the recent shields of central Elysium Planitia and for the ancient shields of Syria Planum and Tempe Terra. The quantity $Q\mu$ (flow rate × viscosity) is derived from adjustment of topographic profiles to the theoretical shape. For the calculation, a constant value for the permeability of 10^{-6} m^2 was assumed.

Values of the product $Q\mu$ correlate with the age of the volcanic regions, with higher values of this product being found for the oldest regions. Independent viscosity estimates at Syria Planum and central Elysium Planitia suggests that the decrease of $Q\mu$ value with time may be influenced by viscosity variations but this idea cannot be confirmed using the other regions on the Tharsis rise. Using these independent viscosity values, it is found that relative effusion rates are homogeneous for a given region, but that there are differences from one region to another. In particular, the shield volcanoes in central Elysium Planitia are characterized by lower viscosity and higher effusion rates. However, the lower viscosity at central Elysium Planitia cannot fully explain the low values of $Q\mu$. Considering the equation of the flow of magma through a dike from the magma chamber to the shield volcano, we suggest that lower volatile contents and deeper magmatic chambers for young volcanism may also contribute to the decrease of $Q\mu$ values with time.

Finally, using a calibration from terrestrial volcanoes (Mauna Loa, Eldborgir and Skjalbreiður), emplacement times of the martian shields were calculated. The calibration assumes that viscosity at Hawaii is similar to the viscosity of the martian volcanoes, with the exception of those of central Elysium Planitia, known to be composed of more fluid lavas. Emplacement times of martian volcanoes may be thus offset if these assumptions are modified. Despite these limitations, emplacement times range froma few hundred thousands of years for Tempe Terra to a few tens of thousands of years for Cerberus tholii. Although
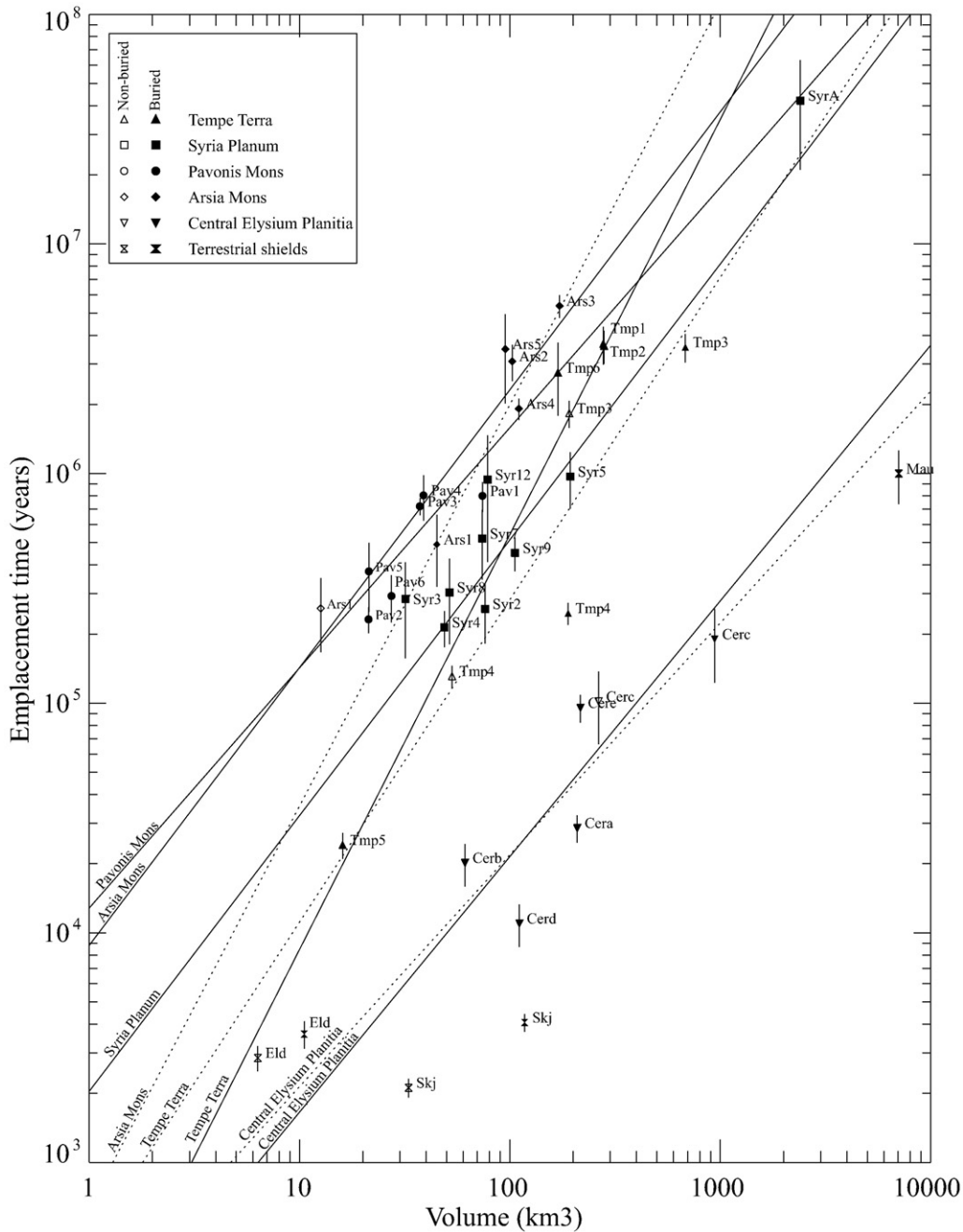
Fig. 18. Relative emplacement times of martian and terrestrial shield volcanoes using the age of the Mauna Loa (1 millions year) as a calibration for the other volcanoes.

one may argue that this simple model relies on several approximations and assumptions, the derived results show an internal consistency, and derived values for the relative effusion rates and emplacement times appear reasonable. This suggests that the development of more advanced physical models for the shape of shield volcanoes could be useful to shed light on lava viscosity, effusion rates, and emplacement time, from geometric characteristics. The differences between the volcanic activity at central Elysium Planitia compared to other regions of Mars raises issues concerning the formation of very fluid lavas in the recent past, and the structure of the present lithosphere that leads to the formation and ascent of such melts.

Acknowledgements

Appendix A. Numerical solution of the shield volcano shape

The shape of the volcano is given as the solution of the following equation:

$$f \frac{d^2 f}{d\eta^2} + \left(\frac{df}{d\eta}\right)^2 + \frac{f}{\eta}\frac{df}{d\eta} + \frac{\eta}{2}\frac{df}{d\eta} = 0 \tag{49}$$

with the two following boundary conditions:

$$\lim_{r \to 0} -\frac{2\pi k\rho g}{\mu} rh\frac{\partial h}{\partial} \to Q_0 \tag{50}$$

$$\eta f \frac{df}{d\eta} \to -\frac{1}{2\pi} \tag{51}$$

A first order numerical scheme was used:

$$f_i\frac{f_{i+1} - 2f_i + f_{i-1}}{\Delta^2} + \left(\frac{f_{i+1} - f_{i-1}}{2\Delta}\right)^2 + \frac{f_i}{\eta_i}\frac{f_{i+1} - f_{i-1}}{2\Delta} + \frac{\eta_i}{2}\frac{f_{i+1} - f_{i-1}}{2\Delta} = 0 \tag{52}$$

where Δ is the interval for η on the discrete grid. After some manipulation the above equation can be written in the explicit form to determine f_{i-1} from f_i and f_{i+1}:

$$f_{i-1}^2 + b f_{i-1} + c = 0 \tag{53}$$

where

$$b = 4f_i - 2f_{i+1} - \eta_i\Delta - \frac{2\Delta f_i}{\eta_i} \tag{54}$$

and

$$c = -8f_i^2 + 4f_i f_{i+1} + f_{i+1}^2 + 2\frac{\Delta}{\eta}f_i f_{i+1} + \eta\Delta f_{i+1} \tag{55}$$

Starting from the flow front, we use the boundary condition:

$$f_{n-1} = f_n + 0.5\,\eta_0\,\Delta \tag{56}$$

where η_0 is the unknown value of the flow front. Then, the second degree equation is solved for each value, from f_{n-2} to f_1, where η_1 is a positive small value as the profile tends to the infinity for $\eta = 0$. The largest solution of the second degree equation is chosen as the height of the volcano increases toward its center. The value of η_0 is optimized such as the boundary condition at the summit is satisfied.

References

Angevine, C.L., Turcotte, D.L., Ockendon, J.R., 1984. Geometrical form of aseismic ridges, volcanoes, and seamounts. J. Geophys. Res. 89 (B13), 11,287–11,292.

Annen, C., 2001. The long-term growth of volcanic edifices: numerical modelling of the role of dyke intrusion and lava-flow emplacement. J. Volcanol. Geotherm. Res. 105, 263–289. doi:10.1016/S0377-0273(00)00257-2.

Baptista, A.R., Mangold, N., Ansan, V., Baratoux, D., Masson, P., Lognonné, P., Williams, D., Bleacher, J.E., Neukum, G., 2008. A swarm of small shield volcanoes on Syria Planum, Mars. J. Geophys. Res. 113, E09010. doi:10.1029/2007JE002945.

Baratoux, D., Mangold, N., Arnald, O., Grégoire, M., Ceuleneer, G., van Ginneken, M., Platevoët, B., Bardintzeff, J.M., Chevrier, V., Pinet, P., Mathé, P.E., 2005. Origins and transport of volcanic sands in Iceland and implications fro the evolution of volcanic material on Mars. XXXVI Lunar and Planetary Science Conference, Houston, TX, USA, p. 1603.

Blasius, K., Cutts, J., 1976. Shield volcanism and lithospheric structure beneath the Tharsis plateau. VII Lunar and Planetary Science Conference, Houston, TX, USA, pp. 3561–3573.

Bleacher, J.E., Greeley, R., 2008. Relating volcano morphometry to the developmental progression of Hawaiian shield volcanoes through slope and hypsometric analyses of SRTM data. J. Geophys. Res. 113, B09208. doi:10.1029/2006JB004661.

Bleacher, J.E., Greeley, R., Williams, D.A., Cave, S.R., Neukum, G., 2007a. Trends in effusive style at the Tharsis Montes, Mars, and implications for the development of the Tharsis province. J Geophys. Res. 112, E09005. doi:10.1029/2006JE002873.

Bleacher, J.E., Greeley, R., Williams, D.A., Neukum, G., 2007b. Morphometric characterization and comparison among the Tharsis Montes-related low shield and fissure vent fields. XXXVIII, Lunar and Planetary Science Conference, Abstact#1314, Houston, TX, USA.

Bonafede, M., Boschi, E., 1992. A porous-flow model of flank eruptions on Mount Etna. J. Volcanol. Geotherm. Res. 49 (3–4), 349–363. doi:10.1016/0377-0273(92)90022-6.

Bonafede, M., Cenni, N., 1998. A porous flow model of magma migration within Mt. Etna: the influence of extended sources and permeability anisotropy. J. Volcanol. Geotherm. Res. 81 (1), 51–68.

Calvari, S., Pinkerton, H., 2004. Birth, growth and morphologic evolution of the Laghetto cinder cone during the 2001 Etna eruption. J. Volcanol. Geotherm. Res. 132, 225–239.

Clague, D.A., and Dalrymple, G.B., 1987. The Hawaiian-Emperor volcanic chain; Part I, Geologic evolution, in Volcanism in Hawaii, edited by R. W. Decker et al., U.S. Geol. Surv. Prof. Pap., 1350, 5 –54.

Davis, P., Tanaka, K., 1993. Small volcanoes in tempe terra, mars: their detailed morphometry and inferred geologic significance. XXIV Lunar and Planetary Science Conference, Houston, TEXAS, USA, p. 379.

Garcia, M.O., Haskins, E.H., Stolper, E., Baker, M., 2007. Stratigraphy of the Hawaii scientific drilling project core (hsdp2): anatomy of a Hawaiian shield volcano. Geochem. Geophys. Geosyst. 8, Q02G20.

Greeley, R., 1992. The Snake River Plain, Idaho: representative of a new category of volcanism. J. Geophys. Res. 87 (B), 2705–2712.

Harris, A.J.L., Allen III, J.S., 2008. One-, two- and three-phase viscosity treatments for basaltic lava flows. J. Geophys. Res. 113, B09212. doi:10.1029/2007JB005035.

Harris, A.J.L., Dehn, J., Calvari, S., 2007. Lava effusion rate definition and measurement: a review. Bull. Volcanol. 70, 1–22.

Hasenaka, T., 1994. Size, distribution, and magma output rate for shield volcanoes of the Michoacfin-guanajuato volcanic field, central Mexico. J. Volcanol. Geotherm. Res. 63, 13–31.

Hauber, E., Bleacher, J.E., Gwinner, K., Williams, D., Greeley, R., 2009. The Topography and morphology of low volcanic shields and associated landforms of plains volcanism in the Tharsis region on Mars. J. Volcan. Geoth. Res. 185, 69–95 (this issue).

Hiesinger, H., Head III, J.W., Neukum, G., 2007. Young lava flows on the eastern flank of Ascraeus Mons: rheological properties derived from High Resolution Stereo Camera (HRSC) images and Mars Orbiter Laser Altimeter (MOLA) data. J. Geophys. Res. 112, E05011. doi:10.1029/2006JE002717.

Hodges, C., Moore, H., 1994. Atlas of volcanic landforms on mars. Technical Report 1534. In U.S. Geological Survey.

Jaeger, W.L., Keszthelyi, L.P., McEwen, A.S., Dundas, C.M., Russel, P.S., 2007. Athabasca Valles, Mars: a lava-draped channel system. Science 317, (1709).

Lacey, A., Ockendon, J.R., Turcotte, D.L., 1981. On the geometrical form of volcanoes. Earth Planet. Sci. Lett. 54 (1), 139–143.

Masson, P., 1980. Contribution to the structural interpretation of the Valles Marineris-noctis labyrinthus-claritas fossae region of Mars. Icarus 30, 49–62.

McGetchin, T.R., Settle, M., Chouet, B., 1974. Cinder cone growth modeled after northeast crater, Mount Etna, Sicily. J. Geophys. Res. 79 (23), 32573272.

Moore, H.J., 2001. Geologic Map of the Tempe-Mareotis Region of Mars, Map I-2727, U.S.G.S., Flagstaff, U.S.A.

Plescia, J., Saunders, R., 1982. Tectonic history of the tharsis region, Mars. J. Geophys. Res. 87, 9775–9791.

Rossi, M.J., 1996. Morphology and mechanism of eruption of post glacial shield volcanoes in Iceland. Bull. Volcanol. 57, 530–540.

Scott, D.R., Stevenson, D.J., 1986. Magma ascent by porous flow. J. Geophys. Res. 91 (B9), 9283–9296.

Sigvaldason, G., Annertz, K., Nilsson, M., 1992. Effect of glacier loading/deloading on volcanism: postglacial volcanic production rate of the Dyngjufjoll area, central Iceland. Bull. Volcanol. 54, 385–392.

Sinton, J., Grönvold, K., Saemundson, K., 2005. Postglacial eruptive history of the western volcanic zone, Iceland. Geochem., Geophys., Geosyst. 6, (Q12009).

Skinner, J., Hare, T.J., Tanaka, K., 2006. Digital renovation of the atlas of mars 1:15,000,000-scale global geologic series maps. XXXVII Lunar and Planetary Science Conference, Houston, TX, USA, abstract 2331.

Tanaka, K., Davis, P., 1988. Tectonic history of the Syria planum province of Mars. J. Geophys. Res. 93 (B12), 14893–14917.

Tanaka, K., Skinner, J., and Trend, M., 2005. Geologic map of the northern plains of Mars, map I-2888, U.S.G.S, Flagstaff, U.S.A.

Turcotte, D., Schubert, G., 2002. Geodynamics, second edition. Cambridge University Press.

Vaucher, J., Baratoux, D., Pinet, P.C., Mangold, N., Ceuleneer, G., Gregoire, M., Daydou, Y., Chevrel, S., Neukum, G., the HRSC Co-investigator team, 2006. Cerberus plains, Mars: chronology of volcanic event and evidence of recent volcanic and tectonic activity. XXXVII Lunar and Planetary Science Conference, Houston, TX, USA, abstract 1851.

Vaucher, J., Baratoux, D., Toplis, M.J., Pinet, P., Mangold, N., Kurita, K., 2009. The morphologies of volcanic landforms at Central Elysium Planitia: Evidence for recent and fluid lavas on Mars. Icarus 200, 39–51. doi:10.1016/j.icarus.2008.11.005.

Vaucher, J., Baratoux, D., Mangold, N., Pinet, P., Kurita, K., Gregoire, M., in revision. The volcanic activity at Central Elysium Planitia: ages, volumes and the relationship with other geologic processes, Icarus.

Wadge, G., Francis, P., 1982. A porous flow model for the geometrical form of volcanoes — critical comments. Earth Planet. Sci. Lett. 57, 453–455.

Wilson, L, Head III, J.W., 1994. Mars: review and analysis of volcanic eruption theory and relationships to observed landforms. Rev. Geophys. 32 (3), 221–263.

Wilson, L., Head, J.W. III, 2002. Heat transfer and melting in subglacial basaltic volcanic eruptions: implications for volcanic deposit morphology and meltwater volumes., in Volcano-ice interaction on Earth and Mars, edited by L. Geological Society, Special publications, pp. 5–26.

Wood, C.A., 1982. On the geometric form of volcanoes — Comment. Earth Planet. Sci. Lett. 57, 451–452.